

Linköping University | Department of Computer and Information Science
Master's thesis, 30 ECTS | Statistics and Machine Learning
2021 | LIU-IDA/LITH-EX-A--2021/001--SE

Reduction of Power Supply Units Hardware Alarms in Radio Base Stations using Machine Learning

Agustín Valencia González

Supervisor : Sanjiv Dwivedi
Examiner : Oleg Sysoev

External supervisor : Oleg Gorbatov, Lackis Eleftheriadis

Upphovsrätt

Detta dokument hålls tillgängligt på Internet - eller dess framtida ersättare - under 25 år från publiceringsdatum under förutsättning att inga extraordinära omständigheter uppstår.

Tillgång till dokumentet innebär tillstånd för var och en att läsa, ladda ner, skriva ut enstaka kopior för enskilt bruk och att använda det oförändrat för ickekommersiell forskning och för undervisning. Överföring av upphovsrätten vid en senare tidpunkt kan inte upphäva detta tillstånd. All annan användning av dokumentet kräver upphovsmannens medgivande. För att garantera äktheten, säkerheten och tillgängligheten finns lösningar av teknisk och administrativ art.

Upphovsmannens ideella rätt innefattar rätt att bli nämnd som upphovsman i den omfattning som god sed kräver vid användning av dokumentet på ovan beskrivna sätt samt skydd mot att dokumentet ändras eller presenteras i sådan form eller i sådant sammanhang som är kränkande för upphovsmannens litterära eller konstnärliga anseende eller egenart.

För ytterligare information om Linköping University Electronic Press se förlagets hemsida <http://www.ep.liu.se/>.

Copyright

The publishers will keep this document online on the Internet - or its possible replacement - for a period of 25 years starting from the date of publication barring exceptional circumstances.

The online availability of the document implies permanent permission for anyone to read, to download, or to print out single copies for his/hers own use and to use it unchanged for non-commercial research and educational purpose. Subsequent transfers of copyright cannot revoke this permission. All other uses of the document are conditional upon the consent of the copyright owner. The publisher has taken technical and administrative measures to assure authenticity, security and accessibility.

According to intellectual property law the author has the right to be mentioned when his/her work is accessed as described above and to be protected against infringement.

For additional information about the Linköping University Electronic Press and its procedures for publication and for assurance of document integrity, please refer to its www home page: <http://www.ep.liu.se/>.

Abstract

Radio Base Stations are one of the most important elements of mobile communication networks, and Power Supply Units are the components that feed them with energy. Thus, by transitivity, Power Supply Units are vital for radio networks. Any malfunctioning in them could be critical and need to be adequately addressed, which might imply high operational costs.

The current work aims to set the ground for improving the mechanisms of how the Radio Base Stations report their Power Supply Units hardware faults to the Network Operations Centre, so they are notified only when the operational continuity is at risk.

A state-of-the-art study has been made regarding power consumptions modelling and forecasting in Radio Base Stations and other domains, finding that *Prophet*, a Generalized Additive Model developed by Facebook, shows promising forecasting capabilities in power demand research in other domains.

At the first stage, time series analysis techniques are applied to preprocess the data to construct a database with uncorrupted information by estimating the process that produced them and then imputing them if there is missing data in any of the features by running a Kalman smoother. Later, these models are also used to forecast the future samples to set a baseline performance.

Secondly, it is estimated the future power consumptions using the *Prophet* model. It is analysed and explained how *Prophet* had been conceived to work, how it learns, and how to use it in an actual application through an example from data of an Radio Base Stations. Its performance is compared against the baselines.

Then, the power consumption is translated into Power Headroom terms, which is the feature of interest for the communications engineers. Then an initial alarm criterion is derived from the critical operational conditions definition.

Finally, the methods are thoroughly tested by running experiments for a set of Radio Base Stations to obtain a more substantial and general overview of the resulting performance of the proposed solution. Showing that *Prophet* achieves an R^2 score of 0.86 in the testing set for an hourly-long-range prediction of three days.

Acknowledgments

`Acknowledgments.tex`

List of Abbreviations

- 3GPP** 3rd Generation Partnership Project
AIC Akaike Information Criterion
API Application Programable Interface
CRITIC Criteria Importance Through Intercriteria Correlation
EENNP Evolutionary Ensemble Neural Network Pool
GAM Generalized Additive Model
GRU Gated Recurrent Unit
HMC Hamiltonian Monte Carlo
LSTM Long Short-Term Memory
MAE Mean Absolut Error
MCAR Missing Completely at Random
MCMC Markov Chain Monte Carlo
MLP Multi-Layer Perceptron
MNO Mobile Network Operator
MOBE Mean Out-of-Bounds Error
NOC Network Operations Centre
NUTS no-U-turn sampler
OBE Out-of-Bounds Error
OSS Operations Support System
PDU Power Distribution Unit
PSU Power Supply Unit
RBS Radio Base Station
RF Random Forest
RMSE Root Mean Square Error
RU Radio Unit
SVR Support Vector Regression

Contents

Abstract	iii
Acknowledgments	iv
List of Abbreviations	v
Contents	vi
List of Figures	ix
List of Tables	xi
1 Introduction	1
1.1 Motivation	1
1.1.1 Context	1
1.1.2 PSU alarms and power headroom	3
1.2 State-of-the-art	5
1.3 Aim	6
1.4 Research questions	6
1.5 Delimitations	6
2 Data analysis	7
2.1 Data acknowledgements	7
2.2 Data description	7
2.2.1 Power supply	7
2.2.2 Radio energy	8
2.2.3 Power distribution	9
2.2.4 Radio traffic	10
2.2.5 Climate	11
3 Theory	13
3.1 Data imputation and database construction	13
3.1.1 Model estimation	13
3.1.2 Notation	14
3.1.3 ARIMA models	15
3.1.4 SARIMA	16
3.1.5 State space representation	16
3.1.6 Structural models	17
3.1.7 Kalman prediction	19
3.1.8 Structural models estimation	19
3.1.9 Kalman smoothing	20
3.2 Prophet forecasting model	21
3.2.1 Trend model	21

3.2.2	Trend forecast	22
3.2.3	Seasonalities	22
3.2.4	Holidays and festivities	22
3.2.5	Hamiltonian Monte Carlo and Prophet fitting	23
4	Methods	24
4.1	Overall pipeline architecture	24
4.2	Database building and time series merging	24
4.2.1	Strategy analysis: Inner join	25
4.2.2	Strategy analysis: Outer join approach	26
4.2.3	Chosen strategy	27
4.3	Auto-ARIMA algorithm	27
4.4	Database construction algorithm	28
4.5	Prophet fitting	29
5	Results	30
5.1	Comparative imputing experiments	30
5.1.1	Unintuitive R^2 values	32
5.1.2	Optim convergence failures	32
5.1.3	Conclusion of the imputing experiments	33
5.2	Forecasting initial experiments	33
5.2.1	Evaluation criteria	33
5.2.2	Baseline predictions models	34
5.2.3	Univariate Prophet model implementation	37
5.2.4	Prophet implementation using exogenous regressors	39
5.2.5	Example forecast performance comparison	41
5.3	Exhaustive forecasting experiments	41
5.3.1	Baselines predictions moving horizon	41
5.3.2	Univariate Prophet prediction moving horizon	42
5.3.3	Multivariate Prophet prediction moving horizon	43
5.3.4	Time performances	44
5.4	Performance summary	44
5.5	Power headroom estimation	45
5.5.1	Power headroom derivation as PSU utilisation complement	45
5.5.2	Criterion considerations	46
5.5.3	Alarm triggering and the n -level safety criteria	47
6	Discussion	48
6.1	Results	48
6.2	Methods	49
6.2.1	Time series merging	49
6.2.2	Time series imputation	49
6.2.3	Forecast	49
6.3	Ethical considerations	50
7	Conclusion	51
8	Future work	52
A	Further results	53
A.1	Baseline predictions	53
A.1.1	Structural time series	53
A.1.2	Auto-ARIMA	54
A.2	Univariate Prophet	55

A.2.1	Training fitting	55
A.2.2	Test predictions	56
A.2.3	Residual analysis	57
A.3	Multivariate Prophet	58
A.3.1	Test predictions	58
A.3.2	Residual analysis	58
A.4	Exhaustive experiments	60
A.4.1	Baselines predictions moving horizon	60
A.4.2	Univariate Prophet prediction moving horizon	61
A.4.3	Multivariate Prophet prediction moving horizon	62
	Bibliography	63

List of Figures

1.1	RBS infrastructure	1
1.2	Different Radio Access Networks architectures	2
1.3	Example of a power infrastructure in an Radio Base Station	3
1.4	Example of variation of a number of connections in a Radio Base Station	4
1.5	Power headroom	4
2.1	Average PSU utilisation example	8
2.2	Standard deviation of Radio Unit voltage example	8
2.3	Average Radio Unit power consumption example	9
2.4	Average Power Distribution Unit voltage example	9
2.5	Connections requests signal example	10
2.6	Data blocks signal example	10
2.7	Active users signal example	11
2.8	Cabinet temperature signal example	11
2.9	Internal and external fan speed signals examples	12
4.1	Overall pipeline architecture	24
4.2	Database consolidation	25
4.3	Inner join	26
4.4	Outer join	27
4.5	Hyndman-Khandakar algorithm for Auto-ARIMA estimation	28
4.6	Database construction algorithm	28
5.1	Comparative imputing experiment pseudocode.	31
5.2	Radio traffic load imputation	31
5.3	Imputation experiments with bad results.	32
5.4	Example of problematic signals for Auto-ARIMA estimation.	32
5.5	Average PSU load signal used for the forecasting experiments	33
5.6	Structural model 3-days baseline overall performance	35
5.7	Structural model 3-days baseline joint distribution	35
5.8	Auto-ARIMA 3-days baseline overall performance	36
5.9	Auto-ARIMA 3-days baseline joint distribution	36
5.10	Training, test and predictions from univariate Prophet	37
5.11	Learnt components from univariate Prophet	38
5.12	Univariate Prophet joint distributions of y and \hat{y}	38
5.13	Training, test and predictions from multivariate Prophet	39
5.14	Learnt components from multivariate Prophet	40
5.15	Multivariate Prophet joint distributions of y and \hat{y}	41
5.16	Baseline predictions performance vs forecast horizon time	42
5.17	Univariate Prophet predictions performance vs forecast horizon time	42
5.18	Multivariate Prophet predictions performance vs forecast horizon time	43
5.19	Multivariate Prophet R^2 vs forecast horizon time	43
5.20	Experiments computing times	44

5.21	Power headroom derivation from PSU Load	46
5.22	Power headroom and discrete availability in percents	47
6.1	Final pipeline architecture	48
A.1	Structural model 3-days baseline predictions	53
A.2	Structural model 3-days baseline residuals	54
A.3	Auto-ARIMA 3-days baseline predictions	54
A.4	Auto-ARIMA 3-days baseline residuals	55
A.5	Training fitting from univariate prophet	56
A.6	Test predictions from univariate Prophet	56
A.7	Univariate prophet residuals	57
A.8	Test predictions from multivariate prophet	58
A.9	Multivariate prophet residuals	59
A.10	Baseline R^2	60
A.11	Baseline MOBE	60
A.12	Univariate moving prediction horizon: R^2	61
A.13	Univariate moving prediction horizon: Mean Out-of-Bounds Error	61
A.14	Multivariate moving prediction horizon: Mean Out-of-Bounds Error	62

List of Tables

5.1	Baselines long-range performance	37
5.2	Prophet's long-range prediction performance example	41
5.3	Mean Absolut Error Summary of models performance by day	44
5.4	Root Mean Square Error Summary of models performance by day	44
5.5	R^2 Summary of models performance by day	45
A.1	Univariate prophet training scores	55
A.2	Univariate prophet prediction performance	57
A.3	Multivariate prophet prediction performance	58

1 Introduction

1.1 Motivation

1.1.1 Context

Mobile communications have shaped how people interact with each other in modern societies. Therefore, it is valid to state that mobile networks are fundamental building blocks for modern lifestyles. Usually, its infrastructure underlies silent and unnoticed. Nonetheless, when they stop working as expected, unpleasant situations, and even chaotic ones, can happen.

Usually, the most visual element of mobile networks for the common eye is the antenna towers. Although, there are several more hardware infrastructure and software that enable communications as we know them.



Figure 1.1: RBS infrastructure. All rights belong to Ericsson

A Radio Base Station (RBS) is the element of telecommunication networks that receives and broadcasts electromagnetic waves to the environment in a determined area and, therefore, one of the essential pieces to enable mobile communications.

Mobile networks are geographically distributed in units called *antenna site* considering multiple cells which comprise more than one cell –usually three–. Depending on its technology, it will vary its components and the architecture in which they are connected, as shown in Figure 1.2. Nonetheless, the main principles stand.

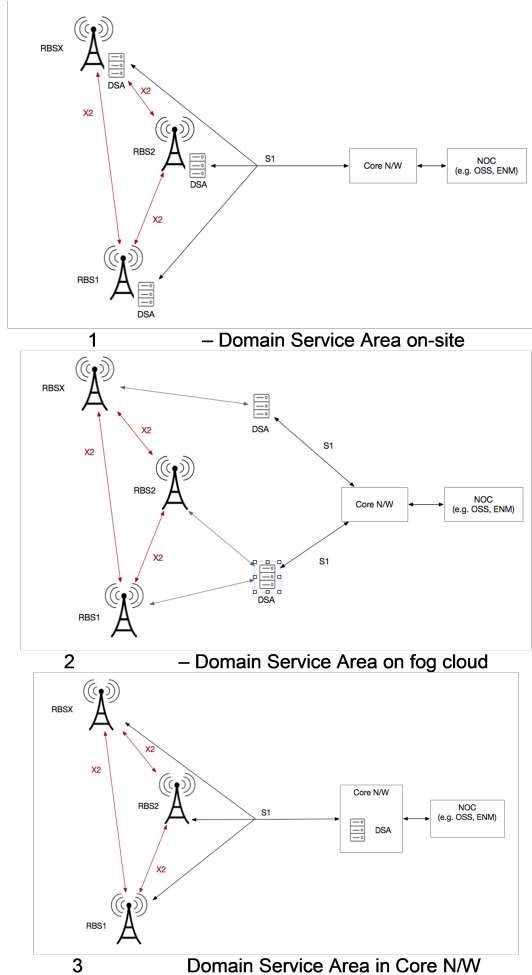


Figure 1.2: Different Radio Access Networks architectures

In present RBSs, in case of any hardware fault, an alarm is triggered and sent to the fault management system (reporting system) and informed to the Operations Support System (OSS) in order to be processed and handled by the Network Operations Centre (NOC). Engineers in the NOC should raise a request to send the field workforce to replace the faulty unit based on the alarm data.

The reality is that not all of the alarms affect the radio performance or degradation of the radio traffic, which implies that there is no urgency in sending service personnel to the RBS site until its operational continuity is at risk.

Setting the right time for sending field workers to the RBS to replace hardware, which sometimes might be located in very isolated or hard to reach locations, would positively affect the maintenance and operational costs for the Mobile Network Operators (MNOs).

As a Statistics and Machine Learning research, the current work does not aim to provide deep knowledge on telecommunications networks. Thus, some communications concepts will not be thoroughly developed, which does not imply any lack of statistical research rigorousness.

1.1.2 PSU alarms and power headroom

The Power Supply Unit (PSU) feeds with power the entire RBS. Nonetheless, usually, one station may contain several PSUs for operational robustness in case of faults, as shown in Figure 1.3. This redundancy implies that when an alarm is received from a PSU, sometimes, there is no need for an immediate replacement of the faulty PSU hardware since the RBS has still enough power available to continue its operation without blackout risk.

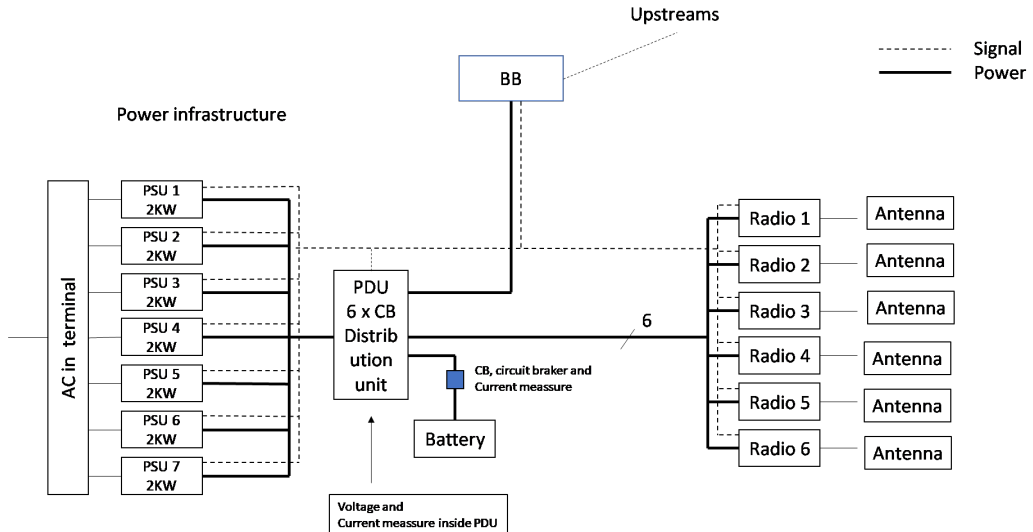


Figure 1.3: Example of a power infrastructure in an RBS¹

Other components to note to understand better the features are the Power Distribution Unit (PDU) which is the unit that manages the power of the system and distributes it according to different operational scenarios. The Radio Units (RUs) are, as its name explains, the units in which the power is converted into electromagnetic waves modulated to carry information and then uses the antennas to broadcast them into the ambient. Last but not least are the power lines, which are not a unit themselves, but interconnects the units so the RBS itself could work as a system. The power lines are the veins that carry the energy to all the elements within the system. Nonetheless, they are not ideal, and power gets dissipated along them. The longer the lines are, the higher the losses related to them.

Added to the power surplus given by redundant PSUs, there is also the fact that they do not use all the available power all the time because the radio traffic has a clear seasonal component as shown in Figure 1.4. Thus, the RUs are not constantly transmitting at their maximum capacity.

¹This is a general overview of the power infrastructure in an RBS, i.e., each station may differ from others depending on how the ad-hoc solution has been designed

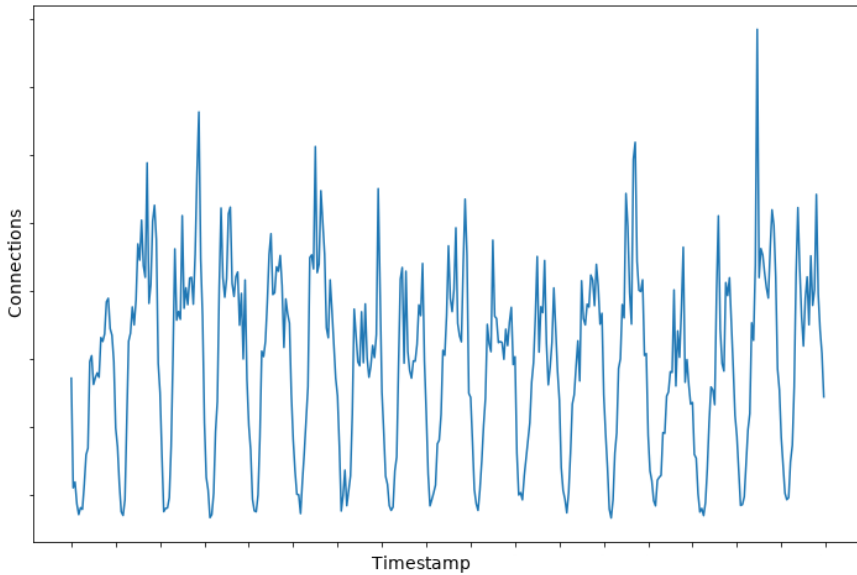


Figure 1.4: Example of variation of a number of connections in a RBS

The *power headroom* P_h , in a new approach for the PSU, then is defined as the difference between the power consumption P_{cons} and the maximum available power P_{max} .

$$P_h = P_{max} - P_{cons} \quad (1.1)$$

Where P_{cons} can be understood as *the consumed power seen from the PSU* [1][2], which will comprise the RUs power consumption, static power consumption, cooling system consumption, the losses in the lines, etc. For simplicity, as this is not a communications thesis, this definition will not be developed in-depth.

In Figure 1.5 it is shown how the amount of PSUs is related to the power headroom and how a decrease in the amount of working PSUs would diminish the power headroom value but still give a reasonable operational margin.

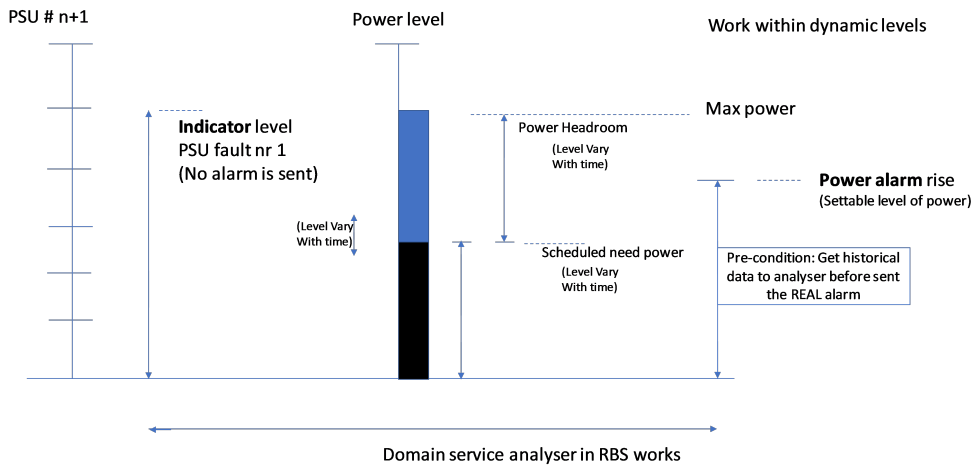


Figure 1.5: Power headroom example

1.2 State-of-the-art

The research on power consumptions in RBSs is not a new topic in the communications community, and they can be seen from two different research perspectives. The first stands from a modelling point of view. It can have a top-to-down approach [3], i.e., focusing on the consumptions first, and based on them, describe the system. Alternatively, there is a bottom-up perspective, in which the overall power consumption of the system is described by the consumptions of each independent building block depending on their different operational modes [4]². Both have in common that they are descriptive works and have constrained their data to pure hardware technologies and their power characteristics. Their primary purpose has been modelling and simulation of communication networks.

The second perspective uses more data than just hardware description. As a consequence, traffic metrics have been shown to be a fundamental covariate to explain power consumption fluctuations in RBSs [5]. Furthermore, STL decomposition has been applied to model the traffic load in RBSs. Then, Holt-Winter's technique [6] has been used to forecast its values, so the power management can adopt power-saving strategies when it is not needed to broadcast at maximum power capacity [7].

When it comes to power consumptions forecast in domains other than communications, the field has also been fruitful. Sensor networks power consumptions using Markov chains [8], power consumptions in data centres using LASSO, elastic-net, Random Forest (RF), KNN, and Multi-Layer Perceptron (MLP) [9], coal-mining power consumption forecast using pure statistics [10] or laser-melting processes using linear regression [11] to mention some.

Furthermore, households power demand forecast is a very fertile domain on its own. Linear regression, decision trees, RF, Support Vector Regression (SVR) and MLP have been applied to predict the demand in northern Morocco [12] finding that MLP performs better than the others, Long Short-Term Memory (LSTM) networks have been applied to learn household consumptions and compared against Gradient Boosting Tree (GBT) and SVR approaches finding that the LSTM model, which they have called *PowerLSTM* outperforms the others[13]. A novel Evolutionary Ensemble Neural Network Pool (EENNP) method is proposed in [14] and applied to power consumptions in western Norway.

The well-used Holt-Winters model has been compared against Facebook's Prophet model in long-range power loads forecast in Kuwait, reaching a MAPE ~ 2% for a prediction horizon of 720 days. Their predictions robustness has been tested by injecting Gaussian noise in different intensities at a fixed (unspecified) forecasting horizon, concluding that Prophet can perform robust power demand predictions while obtaining $R^2 = 0.96$ at a noise intensity of 80% [15]. In the same direction, it has been shown that Prophet performs better than ARIMA models for a long-range of 30 days on power demand prediction using external environmental regressors in an airport in Belgium [16]. In both studies, Prophet's weekly seasonal component is used to recommend the most suitable day of the week to perform maintenance related to power consumptions.

Furthermore, in [17], it has been shown the potential of Prophet for long-range predictions by extending it to work together with a Gated Recurrent Unit (GRU) as an attention layer plus a Criteria Importance Through Intercriteria Correlation (CRITIC) node to weigh both predictions optimally. For a prediction horizon of ~ 6 months, the proposed architecture shows a MAE = 8.5 against to 10.1 and 20.1 from Prophet on its own and ARIMA, respectively.

Thus, the robustness of the predictions made by Prophet models for long-range time horizons makes it an interesting alternative to be applied in communications research. Additionally, it has shown to perform better than standard methods in other fields, which are also highly related to human behaviours. No publication has been found doing so during the research.

²This study considers: power amplifier, analogue frontend, digital baseband, digital control and power system

1.3 Aim

The following work aims to develop a statistical or machine learning method that reports an alarm if and only if the power headroom in a RBS will reach unsafe operational levels based on installed power capacity and power consumption forecasts.

Based on state-of-the-art findings, exploring Prophet's capabilities to also endow of long-range robustness the proposed solution.

1.4 Research questions

1. What is the best way to handle real-world telecommunications and power time series to provide useful structures to mine and learn from them?
2. What are suitable forecast techniques to predict power utilisation in an RBS?
3. Given the power forecast, what are suitable criteria to raise alarms if and only if the RBS operational continuity is at risk?

1.5 Delimitations

Even though one of the overall goals of the present work has been reducing operational costs for MNOs, this has been done without considering the logistics under the maintenance or operational constraints of hardware replacement stock or even RBS geographical location. Therefore, the only factor of operational costs current work tries to optimise is *when* a hardware replacement alarm is raised.



2 Data analysis

2.1 Data acknowledgements

Due to data usage legal restrictions and Ericsson's customers' privacy, internal identifiers used by the company's operations, dates in all timestamps have been anonymised in the thesis to be available for the public domain. Moreover, the data structures and sensitive data values have not been presented in the thesis.

2.2 Data description

The available data is in the form of time series indexed by an RBS unique identifier and the time stamp corresponding to sample time. The data is sparse in different files depending on the domains from where the features have been measured, i.e., the power supply, power distribution, radio traffic, cabinet climate domains, etc. A brief explanation of the information provided by the time series and some random samples from the database are shown in the following subsections. It should be noted that configuration data for base stations is included. This data shows hardware equipment and their settings, for example, the number of PSUs.

2.2.1 Power supply

Power supply interruptions from the Power Grid distribution

This measurement shows how stable the electric power supply from the AC distribution is, i.e., it is a time counter in which the energy supply has been interrupted from the public power distribution. As a consequence, RBS utilise power from other sources such as batteries.

PSU utilisation statistics

PSU utilisation refers to the percentage of PSU's power capacity being consumed by the loads over a determined time. In the available data for this project, this is described by the average, minimum, maximum and standard deviation of these measures over different time durations.

These statistics are, in fact, the most crucial feature in the current work. It can be understood as the complement of the power headroom in per cent. In order to obtain the power values in terms of Watts units, it is needed to know beforehand the installed power capacity.

As there are no direct power headroom measurements, this has been chosen as the target variable, and then the power headroom will be derived from this quantity. In the Figure 2.1, the average of a PSU utilisation is shown as an example.

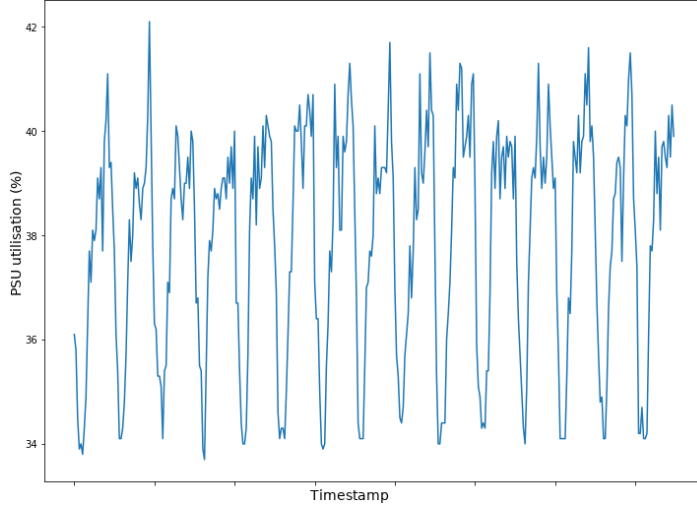


Figure 2.1: Average PSU utilisation example

2.2.2 Radio energy

Radio units voltage statistics

The RUs are fed with energy by the PDU. Nonetheless, this is not a constant and might change over time. The minimum, maximum, average and standard deviation statistics show how these fluctuations have been over a determined time. Figure 2.2 shows the standard deviation of the voltage perceived by the RUs.

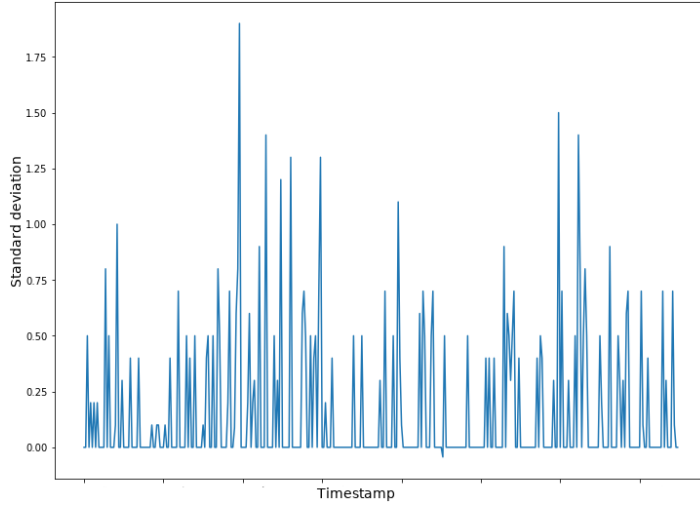


Figure 2.2: Standard deviation of RU voltage example

Radio units power consumption statistics

Supplied energy and power consumption are not the same. Whereas the former refers to the available energy to be used, the consumed power refers to the actual power used for

broadcasting purposes. The minimum, maximum, average and standard deviation statistics have been measured and reported over a determined time. Figure 2.3 presents the average of the consumed power by the RU as an example.

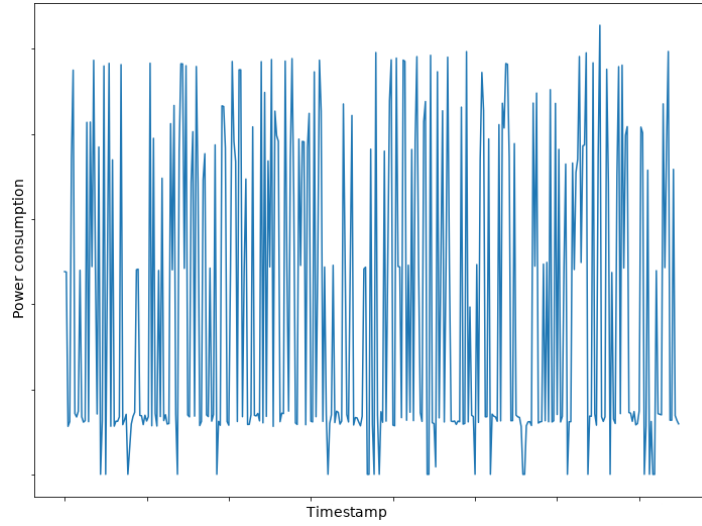


Figure 2.3: Average RU power consumption example

2.2.3 Power distribution

As shown in Figure 1.3, the RUs are not fed directly by the PSUs but by the PDU which manages the different power sources of the RBS. These measurements do not need to be the same as the voltage and power measurements in the RUs because the power lines that connect them could be up to 60 metres long, which might introduce some losses to the system.

Like other features, these are sampled and presented as their minimum, maximum, average and standard deviation over a determined time. Figure 2.4 shows the average of the PDU's output voltage as example.

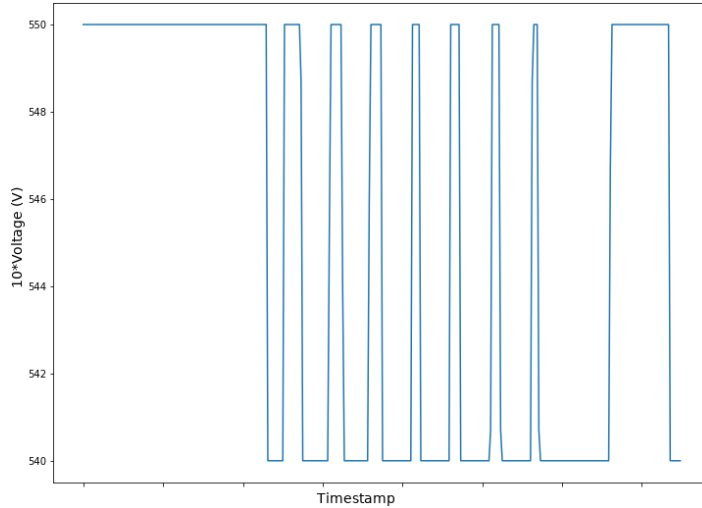


Figure 2.4: Average PDU voltage example

2.2.4 Radio traffic

In the data measured from radio traffic, it is possible to observe the highly seasonal characteristics of users behaviour influenced by the day-night cycle. Examples of data are shown in Figures 2.5, 2.6, and 2.7.

Number of connections

This measurement corresponds to the number of established connections to the radio traffic.

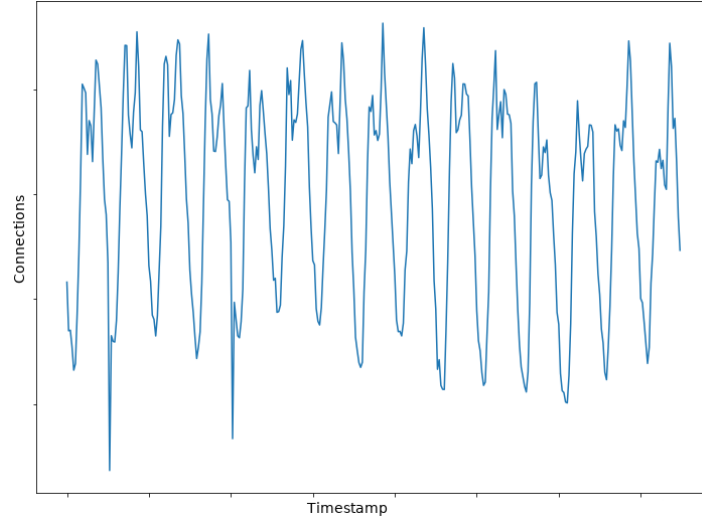


Figure 2.5: Connections requests signal example

Data blocks

This signal corresponds to the number of resource blocks connected to the traffic load in the uplink and downlink.

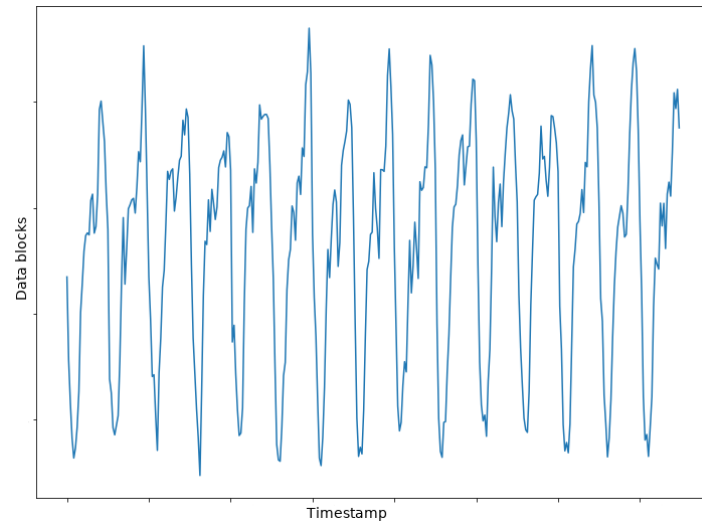


Figure 2.6: Data blocks signal example

Active Users

This feature shows the number of active users connected to the radio traffic load in the uplink and downlink.

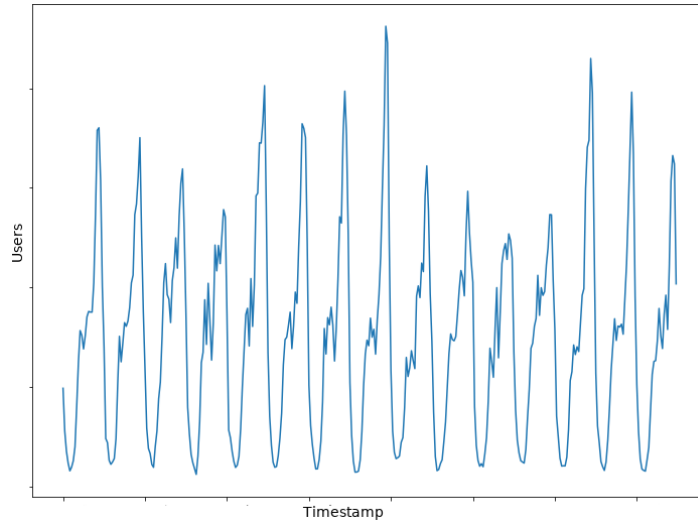


Figure 2.7: Active users signal example

2.2.5 Climate

Average cabinet temperature

In electronic components, high temperature is highly correlated with power dissipation; therefore, its increments in the hardware units will also increase the temperature within the cabinet. An example of average cabinet temperature time series is shown in Figure 2.8.

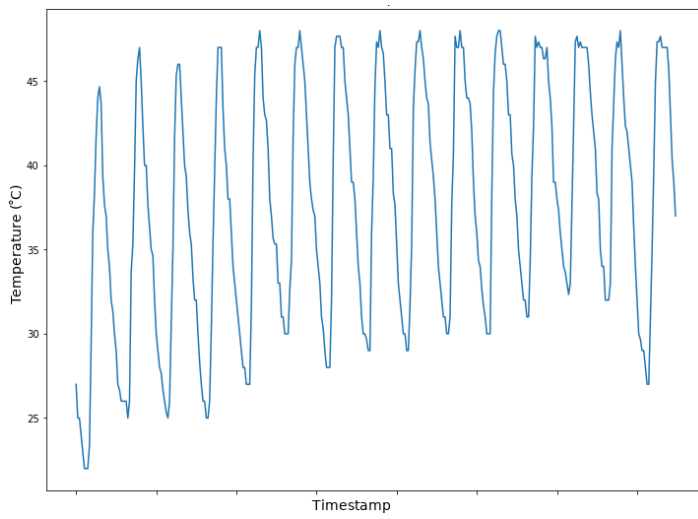


Figure 2.8: Cabinet temperature signal example

Internal and external fan speed

The cabinet is designed to keep the hardware safe. When the cabinet temperature is considered *high*, the fans, one internal and the other external, will be managed to cool down the hardware units. Therefore, the higher the temperature, the faster the fans will run. The reported values correspond to percentages of possible speed values, i.e., a zero value represents a steady fan, whereas a 100 means maximum velocity. Internal and external fan speed signals are shown in Figure 2.9a and 2.9b.

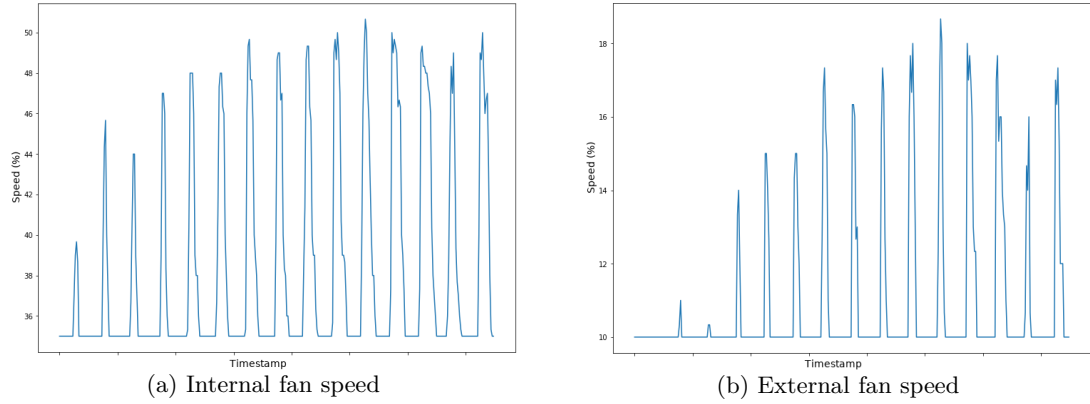


Figure 2.9: Internal and external fan speed signals examples



3 Theory

3.1 Data imputation and database construction

3.1.1 Model estimation

In general, when measuring any variable, there is always a chance of collecting the data and missing some samples. Examples can be people not answering some questions in surveys or incomplete medical records, or even public entities failing to report data or choosing not to disclose it. Sampling data from sensors and reporting it via wireless communication channels is not invulnerable to this type of issues. There can be unforeseen technical issues such as a car crash damaging some units, power blackouts, or even a misconfiguration done by a negligent engineer.

Therefore, handling missing data is a problem that has been under research for a long time. Being Multiple Imputation [18], Expectation-Maximization [19], Nearest Neighbours [20] and hot-deck [21] the most popular techniques to deal with them.

As in the previous step, and based on time constraints, it has been decided not to implement algorithms from scratch but rely on existing known packages to avoid investing in developing time.

Moritz et al. have analysed several univariate time series imputation implementations in R [22], which results later have been compiled in the `imputeTS` R package [23]. Therefore, it is reasonable to rely on their work and use their results to decide which imputing strategy should be taken. Thus, for the current work, the `imputeTS` package will estimate a structural time series model from the data and then perform Kalman smoothing to fill the gaps.

It should be noted that before performing a Kalman smoothing, it is needed to have a state representation of the model, for which `imputeTS` supports Auto-ARIMA state-space estimation and structural time series model fitted by maximum likelihood. In addition, it should be mentioned that the development has been mainly done in python. Nonetheless, for this phase, an R package will be called from python using the `rpy2` module as an interface to bounce between both languages.

3.1.2 Notation

In the following sections, mathematical notations will be used from time series analysis. In order to stand on common ground, notations are defined and explained their meaning.

Backshift operator

The *backshift* (B) or *lag* (L) operators refer to the same operation and both can be found in the literature with no different meaning. In the current work it will , let us define 3.1.1

Definition 3.1.1 (Backshift operator). *Let B denote a backshift or a lag operation in a given series $\{Y_t\} = \{Y_1, Y_2, \dots, Y_n\}$ such that $t, n \in \mathbb{N}, t \leq n$ as*

$$BY_t = Y_{t-1}, \quad t > 1 \quad (3.1)$$

Property 1 (Inverse Backshift). The inverse operation of a lag it is a forward step, thus

$$B^{-1}Y_t = Y_{t+1} \quad (3.2)$$

Property 2. The backshift exponentiation introduced in Property 1 can be generalised to denote back/forward shifts in multiple steps as

$$B^k Y_t = Y_{t-k} \quad (3.3)$$

Property 3 (Backshift algebra). B is a linear operator. Therefore the following is always true.

$$B(aX_t + bY_t + c) = aBX_t + bBY_t + c \quad (3.4)$$

$$B^j B^k Y_t = B^{j+k} Y_t \quad (3.5)$$

Property 4 (Backshift polynomials). The backshift operations can be treated as polynomials to explain more complex expressions.

Let $\{Y_t\} = \{Y_1, Y_2, \dots, Y_n\}$ be a random process and $\boldsymbol{\alpha} = (\alpha_1, \alpha_2, \dots, \alpha_n)$ such that.

$$\begin{aligned} \alpha_{t-1}Y_{t-1} + \alpha_{t-2}Y_{t-2} + \dots + \alpha_{t-k}Y_{t-k} &= \alpha_{t-1}BY_t + \alpha_{t-2}B^2Y_t + \dots + \alpha_{t-k}B^kY_t \\ &= (\alpha_{t-1}B + \alpha_{t-2}B^2 + \dots + \alpha_{t-k}B^k)\{Y_t\} \quad (3.6) \\ &= \alpha(B)\{Y_t\} \end{aligned}$$

The reduction in (3.6) shows the power of the backshift operator, allowing to reduce such large expression into a short and elegant one. Nonetheless, a common flaw in this notation that could create confusion is that it is not needed to specify the polynomial order (k in the example). It can be assumed that whenever the order is not specified is then a general expression for any k -th order polynomial. Nonetheless, whenever its specification is needed, such as to specify an AR or MA model order, a subscript to the notation can be added: $\alpha_k(B)$ in this example.

Difference operator

It is also used the (backward) difference operator used in finite difference calculus to simplify long differences expressions.

Definition 3.1.2 (Difference operator). *Let ∇ denote the difference operator in a given series $\{Y_t\} = \{Y_1, Y_2, \dots, Y_n\}$ such that $t, n \in \mathbb{N}, t \leq n$ as*

$$\nabla Y_t = Y_t - Y_{t-1}, \quad t > 1 \quad (3.7)$$

Property 5 (Difference and backshift operators relation). As an operation between lagged values, it is possible to define ∇ in terms of B

$$\begin{aligned} \nabla Y_t &= Y_t - Y_{t-1} \\ \nabla Y_t &= Y_t - BY_t \\ \nabla Y_t &= (1 - B)Y_t \end{aligned} \quad (3.8)$$

Property 6 (High order differences). Let us obtain the second-order difference as

$$\begin{aligned} \nabla(\nabla Y_t) &= \nabla Y_t - \nabla Y_{t-1} \\ \nabla^2 Y_t &= \nabla Y_t - \nabla BY_t \\ \nabla^2 Y_t &= (1 - B)\nabla Y_t \\ \nabla^2 Y_t &= (1 - B)(1 - B)Y_t \\ \nabla^2 Y_t &= (1 - B)^2 Y_t \end{aligned} \quad (3.9)$$

It can be shown that the development in (3.9) can be extended to the d -th order difference operator having that.

$$\nabla^d Y_t = (1 - B)^d Y_t \quad (3.10)$$

3.1.3 ARIMA models

It is defined that a time series $\{X_t\}$ can be modelled by an *integrated autoregressive moving average* (ARIMA) model if there exist a d -th difference $\{Y_t\} = \nabla^d \{X_t\}$ that can be modelled as an ARMA model [24].

Expanding the definition

$$\begin{aligned} \{Y_t\} &= \nabla^d \{X_t\}, \quad d > 0 \\ &= (1 - B)\nabla^{d-1} \{X_t\} \\ &\vdots \\ &= (1 - B)^{d-1} \nabla \{X_t\} \\ &= (1 - B)^d \{X_t\} \end{aligned} \quad (3.11)$$

Therefore, $(1 - B)^d \{X_t\}$ will be explained by an ARMA(p, q) model if the following recursive equation has a causal and stationary solution:

$$Y_t - \phi_1 Y_{t-1} - \cdots - \phi_p Y_{t-p} = Z_t + \theta_1 Z_{t-1} + \cdots + \theta_q Z_{t-q}$$

Where $\{Z_t\}$ is an uncorrelated noise sequence and ϕ_i and θ_j are the autoregressive and moving-average weights, respectively. Written using backshift operator:

$$\phi(B)\{Y_t\} = \theta(B)Z_t \quad , \quad Z_t \sim \mathcal{N}(0, \sigma^2) \quad (3.12)$$

Replacing 3.11 in 3.12 the ARIMA(p, d, q) process that explains $\{X_t\}$ can be defined as:

$$\phi(B)(1 - B)^d\{X_t\} = \theta(B)Z_t \quad (3.13)$$

Where p is the p -order of the AR(p) process, q the q -order of the MA(q) process and d the successive differencing steps until obtaining a stationary ARMA(p, q) process.

3.1.4 SARIMA

It is said that a time series has a seasonality of period s if $Y_t = Y_{t-s}$. Written using the backshift operator this is $Y_t = B^s Y_t$.

Using the same logical development than for ARIMA derivation, it can be said that $\{Y_t\}$ follows a Seasonal ARIMA (SARIMA) process with period s [24] :

$$\{Y_t\} \sim \text{ARIMA}(p, d, q)(P, D, Q)_s$$

If and only if (3.14) Is a causal ARMA process defined by (3.15).

$$\{X_t\} = (1 - B)^d(1 - B^s)^D\{Y_t\} \quad (3.14)$$

$$\phi(B)\Phi(B^s)X_t = \theta(B)\Theta(B^s)Z_t, \quad \{Z_t\} \sim \mathcal{N}(0, \sigma^2) \quad (3.15)$$

Therefore, replacing (3.14) in (3.15), the SARIMA definition can be rewritten as

$$\phi(B)\Phi(B^s)(1 - B)^d(1 - B^s)^D\{Y_t\} = \theta(B)\Theta(B^s)Z_t, \quad \{Z_t\} \sim \mathcal{N}(0, \sigma^2)$$

Most of the literature obviate a constant c as part of the model since it does not add more insight about the concepts around these derivations. Nonetheless, as it will be seen in the following section it is considered as part of the auto-ARIMA estimation, therefore, the final ARIMA definition in current work is given by:

$$\phi(B)\Phi(B^s)(1 - B)^d(1 - B^s)^D\{Y_t\} = c + \theta(B)\Theta(B^s)Z_t, \quad \{Z_t\} \sim \mathcal{N}(0, \sigma^2) \quad (3.16)$$

Where p, d and q refer to the AR, integral and MA parameters of the ARIMA model, respectively. P, D and Q are the AR, integral and MA parameters of the seasonal construction for the period s .

3.1.5 State space representation

A state-space representation of a time series is suitable for cases in which the underlying nature of a process is hidden and cannot be determined. Nonetheless, indirect observations can be measured.

Thus, state-space representations are given by two equations. The *observation equation* (3.17) relates w -dimensional observable measures as a linear function of the v -dimensional noisy hidden state, and the *state equation* (3.18) determines how the hidden state will transition from time t to $t+1$.

$$\mathbf{Y}_t = G\mathbf{X}_t + \mathbf{W}_t \quad (3.17)$$

$$\mathbf{X}_{t+1} = F\mathbf{X}_t + \mathbf{V}_t \quad (3.18)$$

Where F is a $v \times v$ matrix, G a $w \times v$ matrix, $\{\mathbf{W}_t\} \sim \mathcal{N}(0, R)$, $\{\mathbf{V}_t\} \sim \mathcal{N}(0, Q)$ and $E(\mathbf{V}_s \mathbf{W}_t^T) = 0$ for all t, s .

3.1.6 Structural models

The classical structural models are defined in terms of trend (m), seasonal (s) and noise (ε) components (3.19). Although useful for some applications, they can be too deterministic for some others.

$$X_t = m_t + s_t + \varepsilon_t \quad (3.19)$$

State-space representations allow bringing more flexibility to these components. Therefore, it is natural to extend these concepts to a state-space domain.

3.1.6.1 Local level model

To show how the model is built up, it will be derived by adding component by component from the most straightforward model: the random walk. Let $\{Y_t\}$ be the observable variable from a state-space (3.20) in which the hidden state corresponds is a random variable (3.21), which in fact will determine the *local level model* [24].

$$Y_t = M_t + W_t, \quad W_t \sim \mathcal{N}(0, \sigma_w^2) \quad (3.20)$$

$$M_{t+1} = M_t + V_t, \quad V_t \sim \mathcal{N}(0, \sigma_v^2) \quad (3.21)$$

3.1.6.2 Local linear trend model

It is not difficult to extend this local level model to a *local linear trend model* by adding a slope state B_t .

$$M_t = M_{t-1} + B_{t-1} + V_{t-1} \quad (3.22)$$

Introducing randomness into the slope also:

$$B_t = B_{t-1} + U_t, \quad U_t \sim \mathcal{N}(0, \sigma_u^2) \quad (3.23)$$

As now this model contains multiple state, in order to write the model in state-space form, it can be defined the state vector:

$$\mathbf{X}_t = (M_t, B_t)^T \quad (3.24)$$

Thus, using (3.24), (3.22) and (3.23) can be rewritten as

$$\mathbf{X}_{t+1} = \begin{bmatrix} 1 & 1 \\ 0 & 1 \end{bmatrix} \mathbf{X}_t + \mathbf{V}_t, \quad t = 1, 2, \dots \quad (3.25)$$

Such that

$$\mathbf{V}_t = (V_t, U_t)^T \quad (3.26)$$

The observation equation for the process $\{Y_t\}$ is then by

$$Y_t = [1 \ 0] \mathbf{X}_t + W_t \quad (3.27)$$

Thus, from (3.25) and (3.27) the missing pieces to define the state-space equations are:

$$F = \begin{bmatrix} 1 & 1 \\ 0 & 1 \end{bmatrix} \quad (3.28)$$

$$G = [1 \ 0] \quad (3.29)$$

$$Q = \begin{bmatrix} \sigma_v^2 & 0 \\ 0 & \sigma_u^2 \end{bmatrix} \quad (3.30)$$

$$R = \sigma_w^2 \quad (3.31)$$

3.1.6.3 Noisy seasonal model

Same as the classical structural models, the seasonal component s_t with period d has the properties [25]

$$\begin{aligned} s_{t+d} &= s_t \\ \sum_{t=1}^d s_t &= 0 \end{aligned}$$

Expanding it as in [24] it is obtained that:

$$s_{t+1} = -s_t - \dots - s_{t-d+2}, \quad t = 1, 2, \dots \quad (3.32)$$

From (3.32) it can be constructed a generalised sequence $\{Y_t\}$ by adding a random variable $S_t \sim \mathcal{N}(0, \sigma_s^2)$

$$Y_{t+1} = -Y_t - \dots - Y_{t-d+2} + S_t, \quad t = 1, 2, \dots \quad (3.33)$$

Now, to put it into a state-space form, it is defined the state vector:

$$\mathbf{X} = (Y_t, Y_{t-1}, \dots, Y_{t-d+2})^T \quad (3.34)$$

Therefore the observation equation for $\{Y_t\}$

$$Y_t = [1 \ 0 \ 0 \ \dots \ 0] \mathbf{X}, \quad t = 1, 2, \dots \quad (3.35)$$

$\{\mathbf{X}\}$ in the state equation

$$\mathbf{X}_{t+1} = F \mathbf{X}_t + \mathbf{V}_t, \quad t = 1, 2, \dots \quad (3.36)$$

$$\mathbf{V}_t = (S_t, 0, \dots, 0)^T \quad (3.37)$$

$$F = \begin{bmatrix} -1 & -1 & \dots & -1 & -1 \\ 1 & 0 & \dots & 0 & 0 \\ 0 & 1 & \dots & 0 & 0 \\ \vdots & \vdots & \ddots & \vdots & \vdots \\ 0 & 0 & \dots & 1 & 0 \end{bmatrix} \quad (3.38)$$

3.1.6.4 Structural time series general model

As in (3.19), to construct a general (additive) structural time series model, it is needed to sum each of the components, i.e., the general model is built as a result of merging the linear trend and the noisy seasonal models.

The state vector is then:

$$\mathbf{X}_t = \begin{bmatrix} \mathbf{X}_t^1 \\ \mathbf{X}_t^2 \end{bmatrix} = \begin{bmatrix} (M_t, B_t)^T \\ (Y_t, Y_{t-1}, \dots, Y_{t-d+2})^T \end{bmatrix} = \begin{bmatrix} \begin{bmatrix} M_t \\ B_t \end{bmatrix} \\ \begin{bmatrix} Y_t \\ Y_{t-1} \\ \vdots \\ Y_{t-d+2} \end{bmatrix} \end{bmatrix} \quad (3.39)$$

The state equation

$$\mathbf{X}_{t+1} = \begin{bmatrix} F_1 & 0 \\ 0 & F_2 \end{bmatrix} \mathbf{X}_t + \begin{bmatrix} \mathbf{V}_t^1 \\ \mathbf{V}_t^2 \end{bmatrix} \quad (3.40)$$

Where F_1 and F_2 are the matrices defined in (3.28) and (3.38) respectively. \mathbf{V}_t^1 and \mathbf{V}_t^2 are (3.26) and (3.37).

And the observations equation:

$$Y_t = [1 \ 0 \ 1 \ 0 \ \cdots \ 0] \mathbf{X}_t + W_t \quad (3.41)$$

3.1.7 Kalman prediction

Let $\mathbf{X} = (X_1, \dots, X_v)^T$ be a random vector. Then it can be defined

$$P_t(\mathbf{X}) := (P_t(X_1), \dots, P_t(X_v))^T \quad (3.42)$$

Such that

$$P_t(X_i) := P(X_i | Y_0, \dots, Y_t) \quad (3.43)$$

Is the best linear predictor of X_i in terms of all components of Y_0, Y_1, \dots, Y_t [24]

Then the Kalman one-step predictor for a state-space model given by (3.17) and (3.18) is defined as

$$\hat{\mathbf{X}} := P_{t-1}(\mathbf{X}_t) \quad (3.44)$$

And their error covariance matrices:

$$\Omega_t = E[(\mathbf{X}_t - \hat{\mathbf{X}}_t)(\mathbf{X}_t - \hat{\mathbf{X}}_t)^T] \quad (3.45)$$

The Kalman predictive recursions are then defined by

Initial conditions:

$$\begin{aligned} \hat{\mathbf{X}}_1 &= P(\mathbf{X}_1 | \mathbf{Y}_0) \\ \Omega_1 &= E[(\mathbf{X}_1 - \hat{\mathbf{X}}_1)(\mathbf{X}_1 - \hat{\mathbf{X}}_1)^T] \end{aligned} \quad (3.46)$$

Recursions:

$$\begin{aligned} \hat{\mathbf{X}}_{t+1} &= F_t \hat{\mathbf{X}}_t + \Theta_t \Delta_t^{-1} (\hat{\mathbf{Y}}_t - G_t \hat{\mathbf{X}}_t) \\ \Omega_{t+1} &= F_t \Omega_t F_t^T + Q_t - \Theta_t \Delta_t^{-1} \Theta_t^T \end{aligned} \quad (3.47)$$

Where,

$$\begin{aligned} \Delta_t &= G_t \Omega_t G_t^T + R_t \\ \Theta_t &= F_t \Omega_t F_t^T \end{aligned} \quad (3.48)$$

3.1.8 Structural models estimation

Consider a vector $\boldsymbol{\theta}$ whose components can fully parametrise the state space given by (3.17) and (3.18).

Therefore, it is possible to find $\hat{\boldsymbol{\theta}}_{MLE}$ by maximising the observations in $\{Y_t\}$ with respect to the parameters in $\boldsymbol{\theta}$.

If the conditional probability density of $\mathbf{Y}_t | \mathbf{Y}_{t-1}, \dots, \mathbf{Y}_0$ is $f(\cdot | \mathbf{Y}_{t-1}, \dots, \mathbf{Y}_0)$, then the likelihood can be expressed as

$$\mathcal{L}(\boldsymbol{\theta}; \mathbf{Y}_1, \dots, \mathbf{Y}_n) = \prod_{t=1}^n f(\mathbf{Y}_t | \mathbf{Y}_{t-1}, \dots, \mathbf{Y}_0) \quad (3.49)$$

In general (3.49) is hard to solve. But, if it is assumed that \mathbf{Y}_0 , \mathbf{X}_1 and \mathbf{W}_t , $\mathbf{V}_t, t = 1, 2, \dots$ are *jointly Gaussian*, then the resulting conditional densities will have the form [24]

$$f(\cdot | \mathbf{Y}_{t-1}, \dots, \mathbf{Y}_0) = (2\pi)^{-w/2} (\det \Delta_t)^{-1/2} \exp \left\{ -\frac{1}{2} \mathbf{I}_t^T \Delta_t^{-1} \mathbf{I}_t \right\} \quad (3.50)$$

Where

$$\mathbf{I}_t = \mathbf{Y}_t - P_{t-1} \mathbf{Y}_t = \mathbf{Y}_t - G \hat{\mathbf{X}}_t \quad (3.51)$$

And $P_{t-1} \mathbf{Y}_t$ and $\Delta_t, t \geq 1$ are obtained from the Kalman prediction recursions.

Finally, under the Gaussian assumptions, the likelihood can be rewritten as [24]

$$\mathcal{L}(\boldsymbol{\theta}; \mathbf{Y}_1, \dots, \mathbf{Y}_n) = (2\pi)^{-\frac{n_w}{2}} \left(\prod_{j=1}^n \det \Delta_j \right)^{-\frac{1}{2}} \exp \left\{ -\frac{1}{2} \sum_{j=1}^n \mathbf{I}_j^T \Delta_j^{-1} \mathbf{I}_j \right\} \quad (3.52)$$

Now, for any value of $\boldsymbol{\theta}$, the likelihood values $\mathcal{L}(\boldsymbol{\theta}; \mathbf{Y}_1, \dots, \mathbf{Y}_n)$ can be calculated using the help of Kalman recursions. Thus, in order to find $\hat{\boldsymbol{\theta}}_{MLE}$ it is needed to run some non-linear optimisation algorithm to find the best $\boldsymbol{\theta}$ by maximising \mathcal{L} ¹.

3.1.9 Kalman smoothing

A time series smoothing consists in the estimation of the hidden states \mathbf{X}_t given the complete time series $\mathbf{Y}_1, \dots, \mathbf{Y}_n$ such that $t > n$ [26]. Which is especially suitable when there is any missing data point at a time $t < n$, this is:

$$\mathbf{X}_{t|n} = P_n \mathbf{X}_t \quad (3.53)$$

An the error covariance matrices [24]

$$\Omega_{t|n} = E[(\mathbf{X}_t - \mathbf{X}_{t|n})(\mathbf{X}_t - \mathbf{X}_{t|n})^T] \quad (3.54)$$

Then, the Kalman iterations for the smoothing problem are [24]

$$P_n \mathbf{X}_t = P_{n-1} \mathbf{X}_t + \Omega_{t,n} G_n^T \Delta_n^{-1} (\mathbf{Y}_n - G_n \hat{\mathbf{X}}_n) \quad (3.55)$$

$$\Omega_{t,n+1} = \Omega_{t,n} [F_n \Theta_n \Delta_n^{-1} G_n]^T \quad (3.56)$$

$$\Omega_{t|n} = \Omega_{t|n-1} - \Omega_{t,n} G_n^T \Delta_n^{-1} G_n \Omega_{t,n}^T \quad (3.57)$$

Given the initial conditions in (3.58), which are obtained from the Kalman prediction.

$$\hat{\mathbf{X}}_t = P_{t-1} \mathbf{X}_t \quad (3.58)$$

$$\Omega_{t,t} = \Omega_{t|t-1} = \Omega_t \quad (3.59)$$

¹Constrained to the optimisation algorithm behaviour

3.2 Prophet forecasting model

Prophet is a statistical model developed by engineers at Facebook, which mainly fits its models in Stan and has been open-sourced with public Application Programable Interfaces (APIs) for python and R languages [27]. It takes a regression-fitting approach to learn the time series and then forecasts by extrapolating such models and adding uncertainty in a Bayesian framework.

It uses a decomposable time series models [28] with three main components: trend, seasonality and holidays:

$$y(t) = g(t) + s(t) + h(t) + \varepsilon_t \quad (3.60)$$

Where $g(t)$ is a trend function that models non-periodic fluctuations, $s(t)$ capture different kinds of seasonalities, and $h(t)$ represents special situations that could add irregularities to the other components and a random error term ε .

The model is similar to a Generalized Additive Model (GAM) [29], which allows adding more and more components as needed. The seasonalities are modelled by an exponential smoothing approach [30].

3.2.1 Trend model

Prophet has two trend models: a saturating growth one, which is similar to model population growths in ecosystems [31] and a piecewise model to give the flexibility of trend changes in determined learnt changepoints [27].

The basic saturated growth model is given by

$$g(t) = \frac{C}{1 + \exp\{-k(t - m)\}} \quad (3.61)$$

Where C : Carrying capacity, k : Growth rate, m : Offset parameter

Nonetheless, the saturated growth model in (3.61) does not meet all the usual requirements for some of the applications in which the saturating ceiling varies over time or in which the growth rate is not constant. Therefore, the authors have extended the model as follows.

Let $s_j = 1, \dots, S$ be the number of changepoints where the growth rate is allowed to change. Then, let δ_j be the change rate that happens at s_j , and $\boldsymbol{\delta} \in \mathbb{R}^s$ the vector defined by all δ_j . The growth rate at any time t is then the base rate k plus all the adjustments up to t .

$$k + \sum_{j=1}^{t < s_j} \delta_j \quad (3.62)$$

Expression (3.62) can be rewritten as:

$$k + \mathbf{a}(t)^T \boldsymbol{\delta}$$

Where $a_j = \begin{cases} 1 & , \text{ if } t > s_j \\ 0 & , \text{ otherwise} \end{cases}$ (3.63)

Also, when the growth rate is adjusted, the m needs to be adjusted to ensure continuity.

$$\gamma_j = \left(s_j - m - \sum_{l < j} \gamma_l \right) \left(1 - \frac{k + \sum_{l < j} \delta_l}{k + \sum_{l \leq j} \delta_l} \right) \quad (3.64)$$

Then the linear trend with changepoints is defined by (3.65) piecewise logistic growth model by (3.66) [27].

$$g(t) = (k + \mathbf{a}(t)^T \boldsymbol{\delta}) t + (m + \mathbf{a}(t)^T \boldsymbol{\gamma}) \quad (3.65)$$

$$g(t) = \frac{C(t)}{1 + \exp \{-(k + \mathbf{a}(t)^T \boldsymbol{\delta})(t - (m + \mathbf{a}(t)^T \boldsymbol{\gamma}))\}} \quad (3.66)$$

3.2.2 Trend forecast

After the model has learnt from a history of T time points with S changepoints from which each point has a rate change $\delta_j \sim \text{Laplace}(0, \tau)$.

The trend will keep its last growth rate constant. The forecasts will be made by extrapolating the GAM and simulating samples from $\text{Laplace}(0, \lambda)$ where λ is a variance inferred from the data from the maximum likelihood estimate of the rate scale parameter (3.67).

$$\lambda = \frac{1}{2} \sum_{j=1}^S |\delta_j| \quad (3.67)$$

Once λ has been inferred, the trend forecast and its uncertainty are obtained from

$$\forall j > T \quad , \quad \begin{cases} \delta_j = 0 & \text{w.p. } \frac{T-S}{S} \\ \delta_j \sim \text{Laplace}(0, \lambda) & \text{w.p. } \frac{S}{T} \end{cases} \quad (3.68)$$

3.2.3 Seasonalities

By using the GAM flexibility, it is possible to add different seasonality periods. 365.25 or 7, for yearly and weekly seasonalities, respectively, –in days measurements– for example. These seasonalities are modelled by the use of Fourier series [32].

Therefore, for every given period P , it can be defined that.

$$s(t) = \sum_{n=1}^N \left(a_n \cos\left(\frac{2\pi n t}{P}\right) + b_n \sin\left(\frac{2\pi n t}{P}\right) \right) \quad (3.69)$$

Which has $2N$ params to learn:

$$\boldsymbol{\beta} = [a_1, b_1, a_2, b_2, \dots, a_N, b_N]^T$$

In order to make the structures more manageable, it is defined a matrix of seasonalities comprised of the seasonal vectors for each time step.

$$\mathbf{X}(t) = \left[\cos\left(\frac{2\pi(1)t}{P}\right), \sin\left(\frac{2\pi(1)t}{P}\right), \dots, \cos\left(\frac{2\pi(N)t}{P}\right), \sin\left(\frac{2\pi(N)t}{P}\right) \right] \quad (3.70)$$

Thus, the seasonal component is expressed then as.

$$s(t) = \mathbf{X}(t)\boldsymbol{\beta} \quad (3.71)$$

$$\text{Where } \boldsymbol{\beta} \sim \mathcal{N}(0, \sigma^2) \quad (3.72)$$

3.2.4 Holidays and festivities

Prophet also allows considering non-seasonal events that can significantly affect the forecasts due to changes in peoples behaviour. Namely, Muslim Ramadan, Chinese New Year or the US's Super Bowl.

It is assumed that each holiday is independent. For each holiday i , D_i is the set of past and future dates of it.

Like seasonalities, a regressors matrix is generated indicating whether the time t happens during holiday i and a parameter κ_i to model its influence in the forecast.

$$Z(t) = [\mathbf{1}(t \in D_1), \dots, \mathbf{1}(t \in D_L)] \quad (3.73)$$

$$\therefore h(t) = Z(t)\kappa \quad (3.74)$$

$$\kappa \sim \mathcal{N}(0, \nu^2) \quad (3.75)$$

For practical cases, importing the holidays' dates can be done using the python-holidays open-source package [33]. It is possible also to include other parameters to extend the holiday component to the neighbouring days. For more details, the reader can further investigate in [27].

3.2.5 Hamiltonian Monte Carlo and Prophet fitting

As mentioned, Prophet's core has been implemented in Stan [34]. As a consequence, the R and python APIs work only as intermediaries between the application code and Stan's model definition.

Stan, as a Bayesian framework, uses Markov Chain Monte Carlo (MCMC) algorithms to sample from the defined distributions: Hamiltonian Monte Carlo (HMC) [35] and its adaptive variation no-U-turn sampler (NUTS) [36]. These approaches resemble the Hamiltonian mechanics, which describes the evolution of a system over time, its position q and momentum p , as the partial derivatives of the Hamiltonian function $\mathcal{H}(q, p)$ with respect to the other parameter, i.e., the derivative of the Hamiltonian with respect to the position results in the derivative of the momentum with respect to the time and the same in the opposite sense as defined in (3.76).

$$-\frac{\partial \mathcal{H}}{\partial q} = \frac{dp_i}{dt} \quad (3.76)$$

$$\frac{\partial \mathcal{H}}{\partial p} = \frac{dq_i}{dt} \quad (3.77)$$

Where

$$\mathcal{H}(q, p) = U(q) + K(p) \quad (3.78)$$

Being $U(q)$ the potential energy which is defined to be the negative log-probability density of the distribution for q desired to be sampled (sometimes denoted as θ in Bayesian literature), and $K(p)$ the negative log-probability density of multi-normal $\mathcal{N}(0, \Sigma)$ [37].

The HMC iterations consist of two steps. In the first step, samples for the momentum variables are drawn from their multi-normal distribution. In the second step, it is used Leapfrog numerical integration [38] to solve the Hamiltonian equations to run a Metropolis-Hastings accept/reject step later to propose a new state of the system.

It should be noted that for maximum a posteriori estimation, it is used Limited-memory-Broyden–Fletcher–Goldfarb–Shanno algorithm (L-BFGS) optimisation method [39]. L-BFGS is an iterative method for solving unconstrained nonlinear optimisation problems using a limited amount of computer memory.

4 Methods

4.1 Overall pipeline architecture

By joining all the parts exposed in the previous chapters, the resulting pipeline proposed as a solution is shown in Figure 4.1. Based on the flow presented, the obtained results are summarised in the following sections.

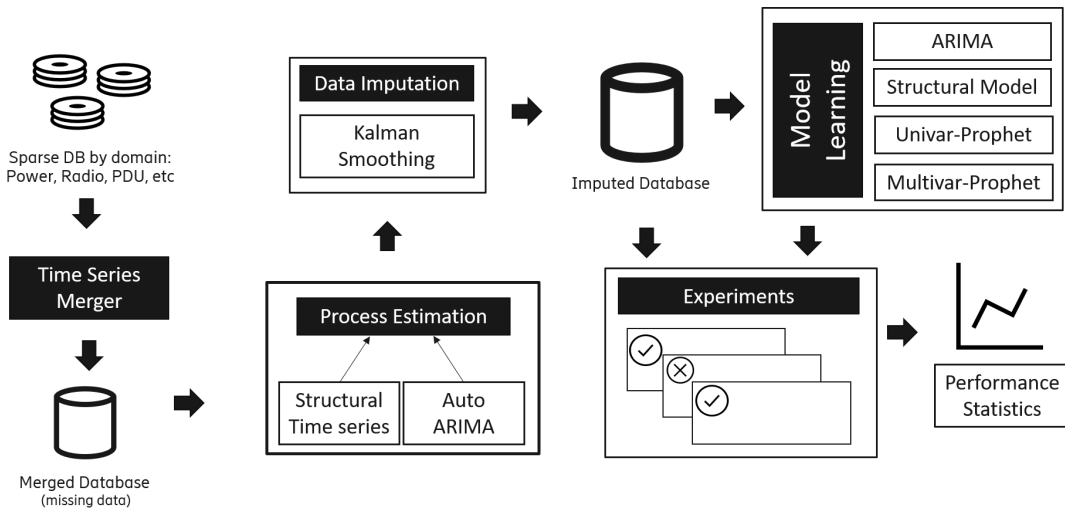


Figure 4.1: Overall pipeline architecture

4.2 Database building and time series merging

As mentioned, the data is sparse across several files depending on its domain. Therefore, all the data has been merged into one consolidated database to make it more manageable to handle.

There is, then, the problem of deciding the best approach to join all these data without corrupting its integrity as valid time series for the present research; this means having an invariant sampling time with fully defined observations vectors.

Among the data tables, it can be seen that the two fields that are always present, and therefore are suitable to use as keys to index all the different tables and join them, are the timestamp of the sample and the RBS from where it comes from. Therefore, the tuples $(date_i, rbs_i)$ will be used as keys

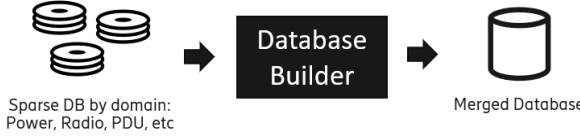


Figure 4.2: Database consolidation

This means, having two relations $R(x_1, \dots, x_n)$ and $S(y_1, \dots, y_m)$ a third relation could be constructed $Q(z_1, \dots, z_k) = R \times S$ such that $R(\vec{x}_i) = S(\vec{y}_i)$ be the keys [40].

In an ideal situation, all the time series for a given RBS would have no missing data and identical timestamps, so just intersecting them would result in a complete-time series with equal sampling time, and no information would be lost.

Nonetheless, that is not the current case. As real-world data, technical issues happen now and then, and there are missing samples or the timestamps between different files are not exactly the same, and therefore, a join using them will not perform as expected.

The present work has been implemented mainly in Python with a few exceptions in R. The joining part is not an exception; thus, pandas `merge` options are available to use: *left*, *right*, *outer*, *inner* or *cross*. Merge operations in pandas work on two sets [41]. Thus, for joining multiple series, successive two-sided `merge` operations have to be performed.

4.2.1 Strategy analysis: Inner join

An inner join constitutes an intersection between both sets. The implementation in pandas allows indicating the keys to be intersected, and as a result, it is returned a tuple containing the matched keys with the remaining members.

This can be expressed as the following

$$Q(date_i, rbs_i, x_{i_1}, \dots, x_{i_n}, y_{i_1}, \dots, y_{i_m}) = \\ R(date_i, rbs_i, x_{i_1}, \dots, x_{i_n}) \cap S(date_i, rbs_i, y_{i_1}, \dots, y_{i_m})$$

Furthermore, in a more programming-friendly fashion, it can also be expressed as a SQL query. The expression above would be as the following and graphically as a 3D Venn diagram as in 4.3.

```

1 SELECT *
2 FROM R
3 INNER JOIN S
4 ON R.date = S.date AND R.rbs = S.rbs;

```

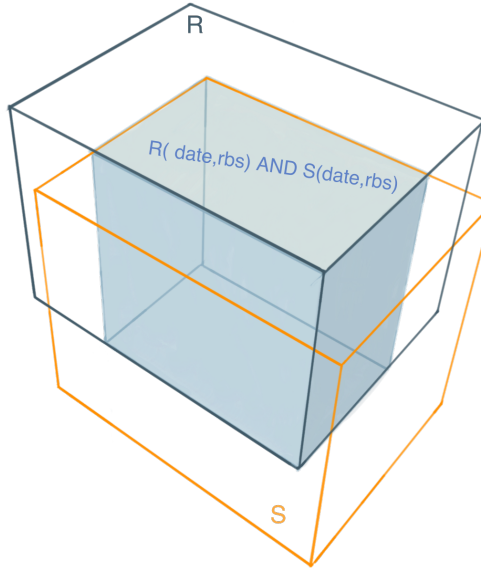


Figure 4.3: Inner join

The biggest drawback of this approach relies on losing the observations that do not have overlapping dates which is a situation to avoid.

4.2.2 Strategy analysis: Outer join approach

Whereas an inner join implies an intersection, an outer join can be understood as a union.

In pandas implementation, a union is performed in the keys domain, and the rest of the vector is preserved. If there is some missing value in terms of samples or the full features, `NaN` will be used to fill in.

Given the relations R and S

$$R(date_i, rbs_i, x_{i_1}, \dots, x_{i_n}), S(date_i, rbs_i, y_{i_1}, \dots, y_{i_m})$$

The resulting *outer-joined* relation Q on keys $(date_i, rbs_i)$

$$Q(date_i, rbs_i) = R(date_i, rbs_i) \cup S(date_i, rbs_i)$$

Such that the missing values on each of the relations are declared as `NaN`

$$Q(x_i) = \text{NaN}, \forall R(y_i) : (date_i, rbs_i) \in R \wedge (date_i, rbs_i) \notin S$$

$$Q(y_i) = \text{NaN}, \forall S(x_i) : (date_i, rbs_i) \in S \wedge (date_i, rbs_i) \notin R$$

Again, in a more programming-friendly fashion, the SQL query would look like the following and a more explanatory Venn diagram as in 4.4.

```

1 SELECT *
2 FROM R
3 FULL OUTER JOIN S
4 ON R.date = S.date AND R.rbs = S.rbs;
```

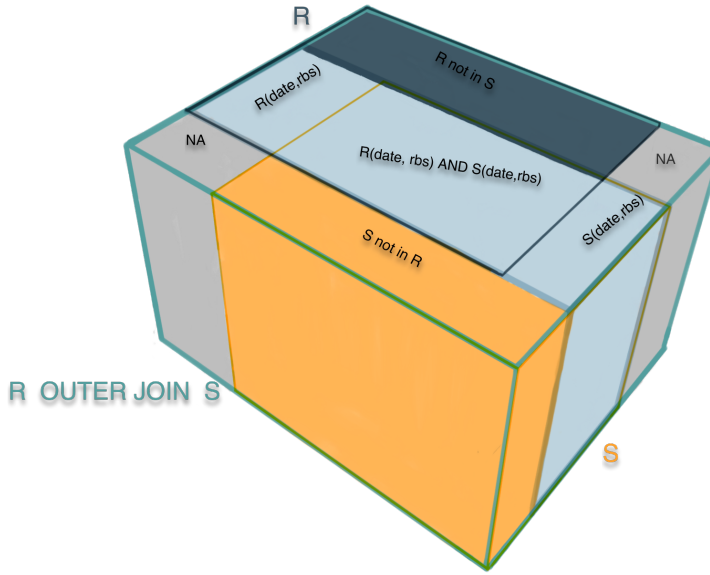


Figure 4.4: Outer join

The drawback of this approach is related to its NaNs insertions, which will imply either postprocessing after merging all the time series or preprocessing before the learning stage.

4.2.3 Chosen strategy

Given the analysis, it has been decided that not losing information is more important than having to process it later to handle the non-computable values. Therefore, the outer join approach will be used for the following steps.

4.3 Auto-ARIMA algorithm

Despite the fact that in the library the procedure is called *auto-ARIMA*, it does also support SARIMA models.

The main goal of auto-tuning these models is to choose the appropriate p, q, d, P, Q and D values so the model can make a good approximation of the process. If d and D are known, p, q, P, Q can be selected by using an information criterion such as the Akaike Information Criterion (AIC) [42]:

$$\text{AIC} = -2 \log(L) + 2(p + q + P + Q + k) \quad (4.1)$$

Where $k = 1$ if $c \neq 0$ in equation (3.16) and 0 otherwise, and L is the maximised likelihood of the model fitted to $(1 - B)^d(1 - B^s)^D\{Y_t\}$ [43].

`ImputeTS` library does not implement the (S)ARIMA estimation on its code. Instead, it uses the `forecast` package to do for it [23].

The `forecast` library implements the Hyndman-Khandakar algorithm for 3.16, which uses an heuristic that combines unit root tests, AIC minimisation and MLE maximisation as shown in Figure 4.5 [43].

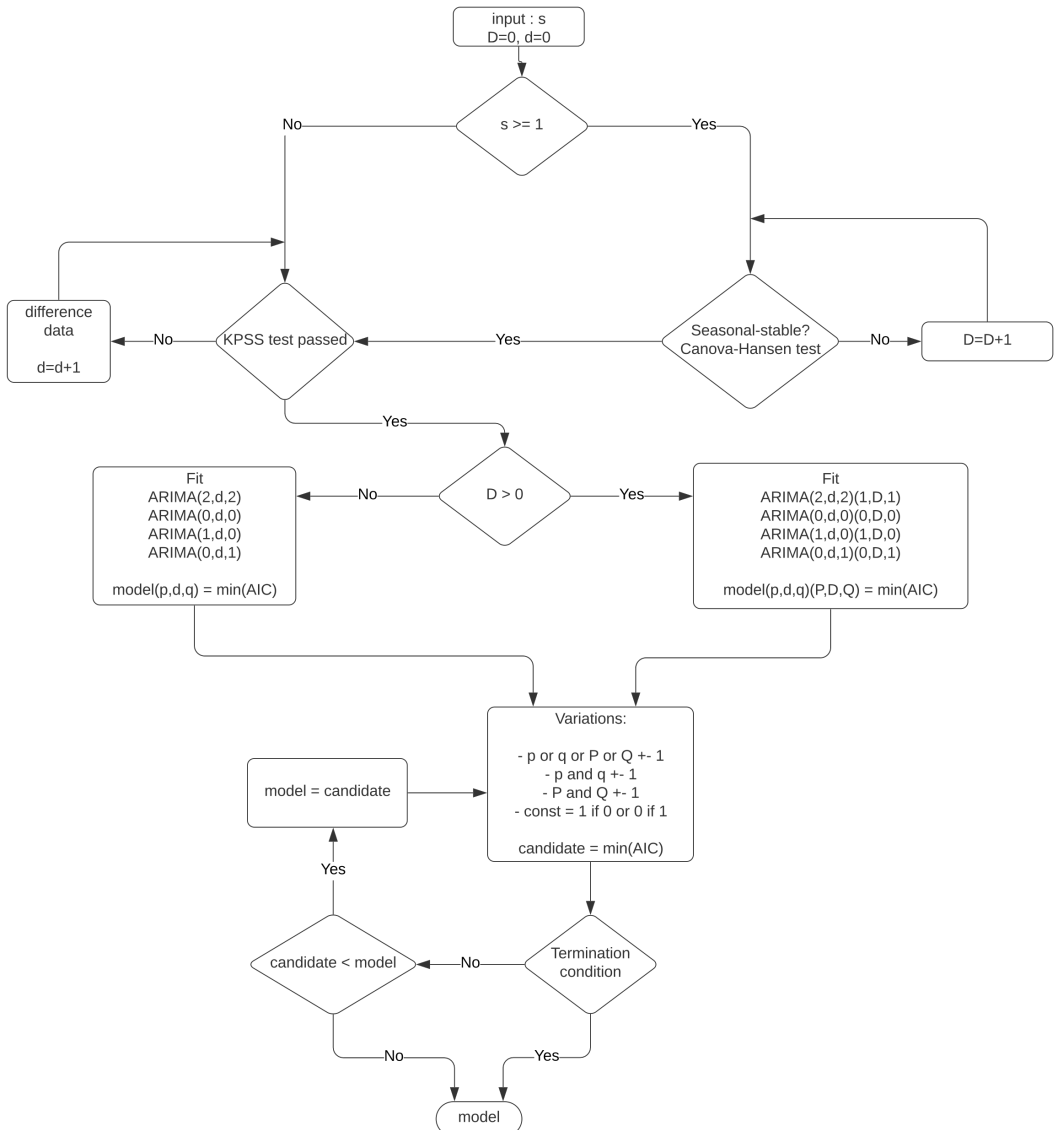


Figure 4.5: Hyndman-Khandakar algorithm for Auto-ARIMA estimation

4.4 Database construction algorithm

It has been implemented a pipeline to build a unified and non-corrupted database from the sparsed raw files so that the forecasting section could learn from reliable data.

In Figure 4.6, it is shown how the implemented blocks interact with each other to accomplish this task.

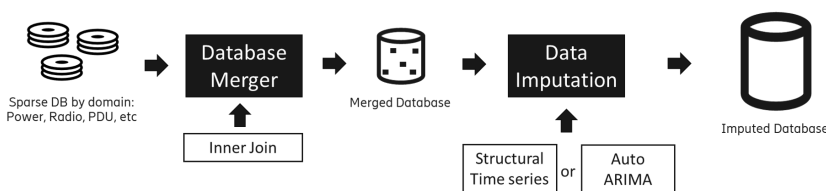


Figure 4.6: Database construction algorithm

4.5 Prophet fitting

Prophet's Stan core [34] can be found in their github repository¹ for further detailed research.

The API expose several more parameters to tune the models beyond the ones explained in Chapter 3. Some of them refer to the amount of MCMC samples used to fit the trend, the limit of trend changepoints, the confidence interval size or some regularization variables used in the Stan model among others.

Another handy feature that allows using GAMs is the ability to plot each component on its own, which allows the analyst to spot abnormalities when debugging a model. These plots will be shown and explained in Chapter 5.

¹<https://github.com/facebook/prophet>



5 Results

5.1 Comparative imputing experiments

A set of thorough experiments has been designed to compare both model estimation techniques and empirically determine which one performs better for the current dataset.

The starting point is a database containing approximately two months of measurements from several RBSs. Then, the database is mined to find $n = 50$ signals per feature with no missing data. After that, it has been artificially removed a given ratio of data using a uniform distribution so that it can be simulated a Missing Completely at Random (MCAR) scenario [44].

The two algorithms run to estimate the process models and use them to run the Kalman smoothing. It is used the coefficient of determination R^2 to compare the performance of the models.

$$R^2 = 1 - \frac{\sum_i (y_i - \hat{y}_i)^2}{\sum_i (y_i - \bar{y})^2} \quad (5.1)$$

Where y_i refers to the i -th data sample, \hat{y} its estimated value and \bar{y} the series mean.

Thus, having perfect predictions would cancel-out the numerator of the right-hand term and produce a score equal to 1. Therefore, the closer the score is to 1, the better quality has been the data imputation.

The process of removing-data, imputing and computing the coefficient of determination value, is performed iteratively while increasing the amount simulated missing data, then the mean of the R^2 values from the n selected RBS are reported.

In Figure 5.1, it is shown the experiment's algorithm pseudocode in order to give more context of the meaning of the results plots.

```

1 input : database, ratio_step, ratio_min, ratio_max
2 output: mean_scores
3
4 let n ← rbs batch size
5 let grid ← [ratio_min : ratio_step : ratio_max]
6 let mean_scores ← []
7
8 foreach feature in database.get_features() do:
9     sites ← database.get_random_sites(n)
10    i ← 0
11    foreach ratio in grid do:
12        let arima_scores ← []
13        let structural_scores ← []
14        j ← 0
15        foreach site in sites do:
16            data ← database.get_site_data(site, feature)
17            sim_data ← remove_uniform_random_data(data, ratio)
18
19            imputed_arima ← impute_with_arima(sim_data)
20            imputed_structural ← impute_with_structural_model(sim_data)
21
22            arima_scores[j] ←  $R^2$ (data, imputed_arima)
23            structural_scores[j] ←  $R^2$ (data, imputed_structural)
24            j ← j + 1
25            mean_scores[i] ← (ratio, mean(arima_scores), mean(structural_scores))
26            i ← i + 1
27
return mean_scores

```

Figure 5.1: Comparative imputing experiment pseudocode.

Figure 5.2 shows the results of the imputation comparison for the radio traffic as example. It can be seen that the R^2 value decreases, as expected, when the missing data ratio increases. It also can be seen that in this example, and in most of them, structural models performs better than ARIMA models for imputing.

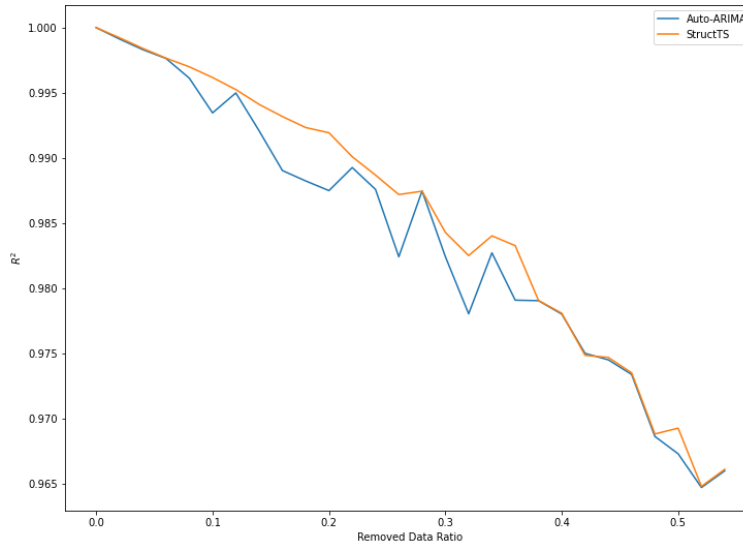


Figure 5.2: Radio traffic load imputation

Although it was obtained very promising results for some of the imputed signals, there were other cases where the experiment did not perform as expected. In the following subsections, they will be discussed.

5.1.1 Unintuitive R^2 values

There are cases in which Auto-ARIMA estimation shows poor and even negative R^2 values as shown in Figure 5.3. These are unintuitive results, as R^2 values are usually expected to be limited to the $[0, 1]$ interval.

Nonetheless, this is meant only for linear models, where the worst fitted model is assumed to be the observations mean [45]. Thus, having negative R^2 values implies that the observations mean explains more variance than the fitted model.

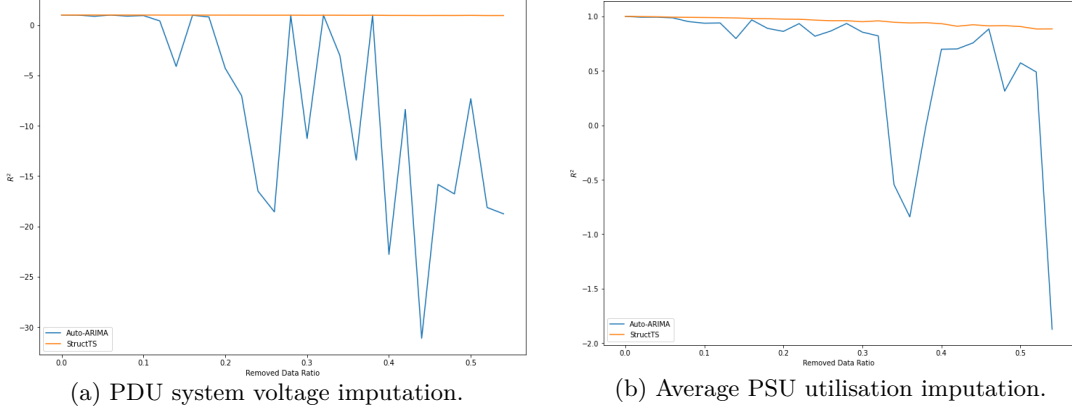


Figure 5.3: Imputation experiments with bad results.

5.1.2 Optim convergence failures

The model estimation threw runtime exceptions for some features due to the R code calls to the `optim` library not converging. These exceptions were found to be an actual bug in the library that occurs when the function being optimised tends to a constant value as shown in Figure 5.4. A dedicated routine was written to catch whenever this exception was thrown and run a simple interpolation instead of estimating the model.

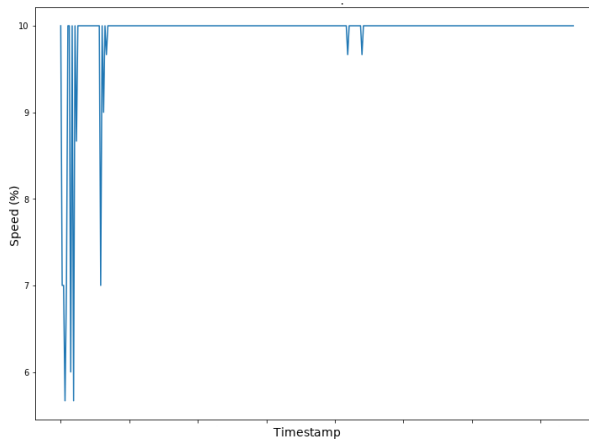


Figure 5.4: Example of problematic signals for Auto-ARIMA estimation.

5.1.3 Conclusion of the imputing experiments

As the ARIMA imputation has shown to be unstable for some signals. Even though that for the same signals the structural model do not overperform either, stills better than very negative R^2 scores. In conclusion, based on this experiment's results, the structural models approach has been the chosen methodology to impute the missing data and construct the database.

5.2 Forecasting initial experiments

The average PSU load signal shown in Figure 5.5 has been chosen to run the following experiments. It is not a particularly easy signal since it contains some severe outliers in the first days that turned the power to almost zero, and at the end, the average power consumption seems to decrease.

It is necessary to notice that in every forecasting model, the longer the prediction horizon is, the more uncertainty and thus the lower performance. For this experiment, it has been decided to leave the last 10% of data for testing purposes.

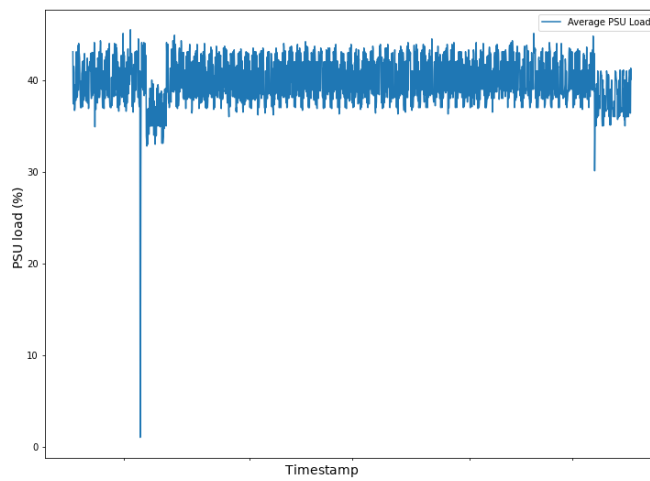


Figure 5.5: Average PSU load signal used for the forecasting experiments

In the following sections, it is going to be shown first a pure univariate approach and later it will be added more exogenous regressors to improve the predictions. The models will be evaluated by using the scores described in Section 5.2.1.

5.2.1 Evaluation criteria

Coefficient of determination

As previously mentioned, the coefficient of determination R^2 is a measure of how many variance of \hat{y} is explained by the variance in y in a linear regression context. It is compared against the considered *worst possible linear approximation* which corresponds to the samples mean.

Although the current application is not a linear regression case, R^2 is still considered a valuable score to compare predictor performances, nonetheless, as the linearity assumption is not met, its values would reside in $(-\infty, 1]$ where 0 still being the mean value, but it is no longer considered the worst possible fit.

$$R^2 = 1 - \frac{\sum_i (y_i - \hat{y}_i)^2}{\sum_i (y_i - \bar{y}_i)^2} \quad (5.2)$$

Mean absolute error

It measures, in absolute terms, the deviations from the true values. Mean Absolute Error (MAE) is preferred, given its interpretability, over Root Mean Square Error (RMSE) [46].

$$\text{MAE} = \frac{1}{N} \sum_{i=1}^N |y_i - \hat{y}_i| \quad (5.3)$$

Mean out-of-bounds error

As a result of the fitting process, prophet's output is comprised by the mean prediction \hat{y}_t and also its lower and upper boundaries for a given confidence value when constructing the predictor object which defaults at 80%

Let then the Out-of-Bounds Error (OBE) be the out-of-the-confidence-bands error defined by (5.4) where $\Delta\hat{y}_t$ is the computed confidence interval half-magnitude for the time t . Then the Mean Out-of-Bounds Error (MOBE) can be obtained by taking the mean of these values to obtain an overall performance score as in (5.5).

$$\text{OBE}_i = \min \left\{ |y_i - (\hat{y}_i - \Delta\hat{y}_i)|, |y_i - (\hat{y}_i + \Delta\hat{y}_i)| \right\} \quad (5.4)$$

$$\text{MOBE} = \frac{1}{N} \sum_{i=1}^N \text{OBE}_i \quad (5.5)$$

5.2.2 Baseline predictions models

For the imputation step, it has been learnt the seasonal ARIMA and structural models to fill the missing values by applying Kalman smoothing algorithm. Furthermore, these models can also be used to forecast the future observations.

They are not expected to highly perform, nonetheless, predicting with them can be used as benchmark to compare other models' improvements over their baseline.

Structural model predictions

In Figure 5.6, it is shown the overall performance of the structural time series predictor. It can be seen that its predictive mean tends to also follows the test dataset mean, whereas the confidence interval is wider the further the prediction horizon is. In A.1.1 more in detail plots are available for the reader without collapsing the main text of the report.

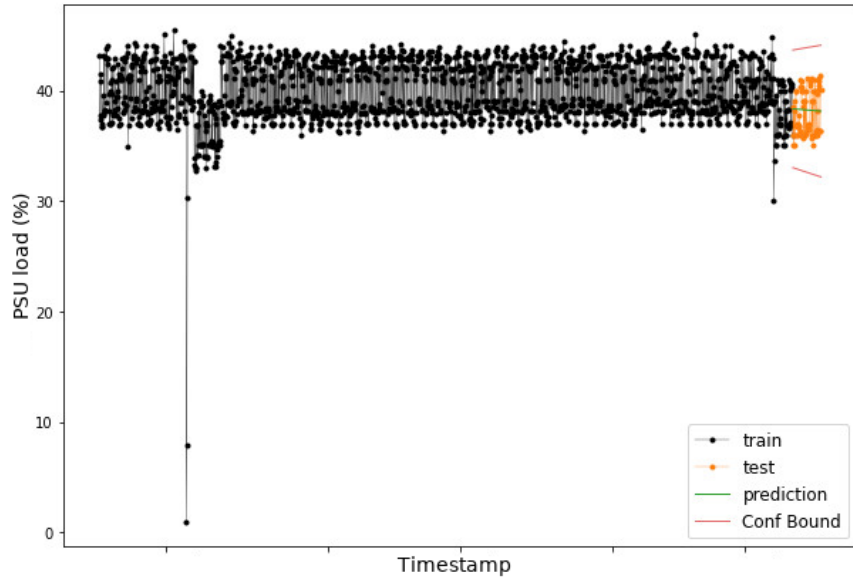


Figure 5.6: Structural model 3-days baseline overall performance

When plotting how the predictions \hat{y} and the real values y are distributed, the ideal prediction would be denoted by the positive unitary line. Therefore, the results in Figure 5.7 can be considered very poor.

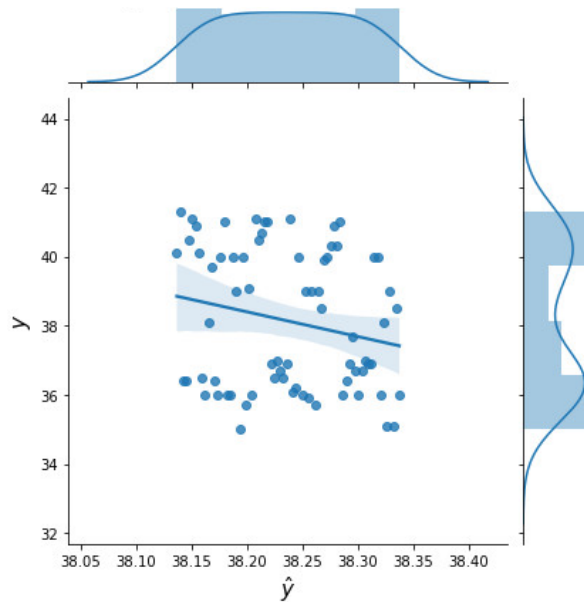


Figure 5.7: Structural model 3-days baseline joint distribution

Auto-ARIMA implementation

Same as in Section 5.2.2, an Auto-ARIMA model is trained and used to make predictions. In this case, it can be seen that, in the short range, the predictive mean tries -poorly- to follow the actual data fluctuations. But later, in the long range just tends to the data mean. In appendix A.1.2 can be found more detailed plots of the results

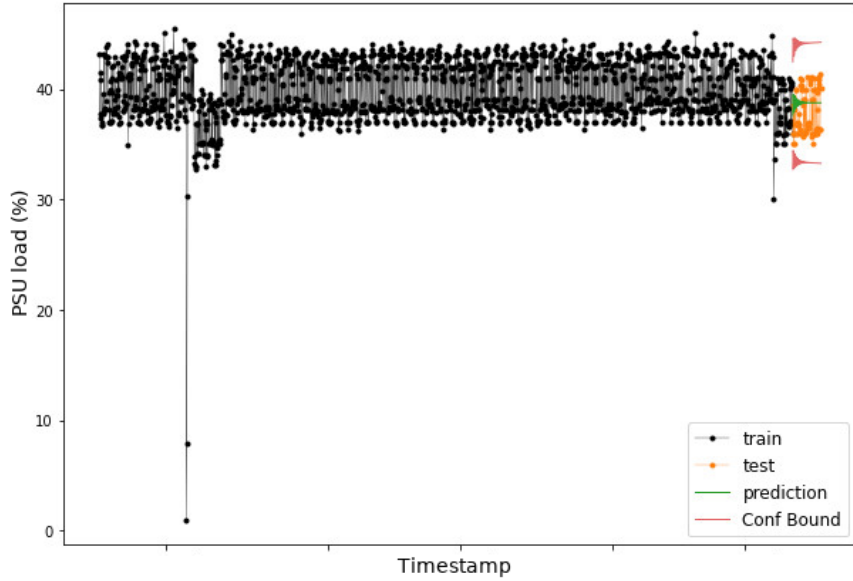


Figure 5.8: Auto-ARIMA 3-days baseline overall performance

Although the joint distribution of predictions and true values has been slightly improved, stills very poor.

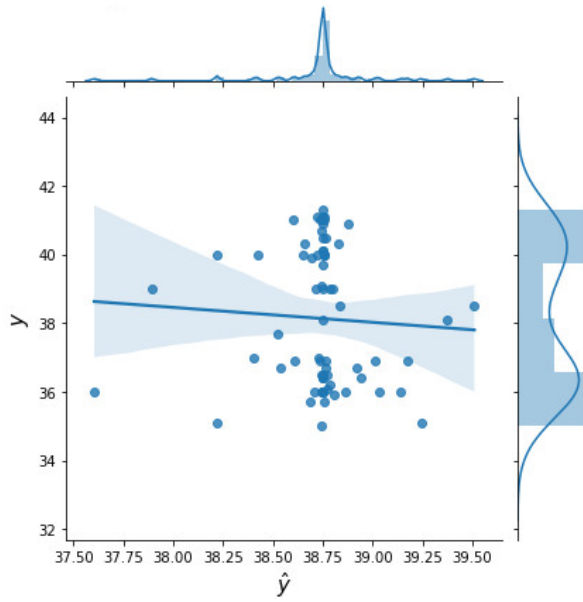


Figure 5.9: Auto-ARIMA 3-days baseline joint distribution

Overall baselines scores

In Table 5.1, it is summarised the long-range prediction of both baselines. They perform very poorly, nonetheless, as naive baselines, it is not expected any other outcome.

Score	Structural Model	Auto-ARIMA
MAE	1.87	1.95
R^2	-0.02	-0.12
MOBE	0	0
RMSE	2.02	2.12

Table 5.1: Baselines long-range performance

5.2.3 Univariate Prophet model implementation

Figure 5.10 shows the complete results of training and testing for a univariate Prophet model. In comparison to the baselines, now it can be observed that the prediction mean tends to follow a more clear seasonal pattern, nonetheless in the testing set it appears to miss the trend change.

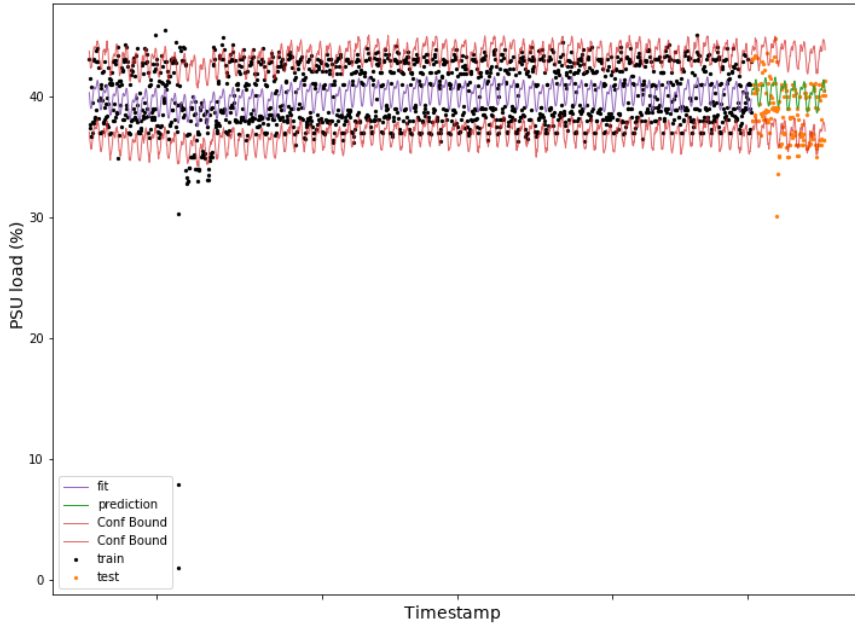


Figure 5.10: Training, test and predictions from univariate Prophet

More detailed plots can be found in Appendix A.2.

Model learnt components

Figure 5.11 presents the learnt approximation of every component in the GAM. Although the trend did not overfit to the outliers, still learnt that there is a break point and changed the piecewise trend.

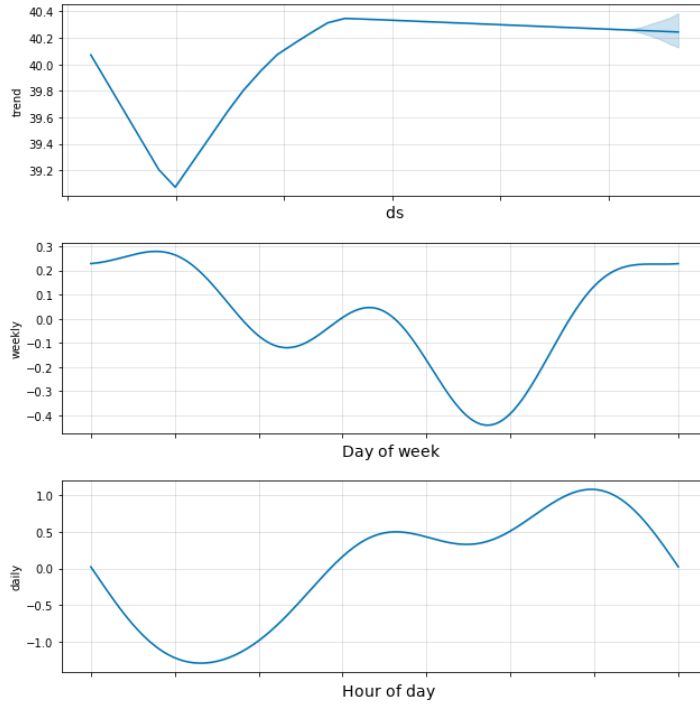
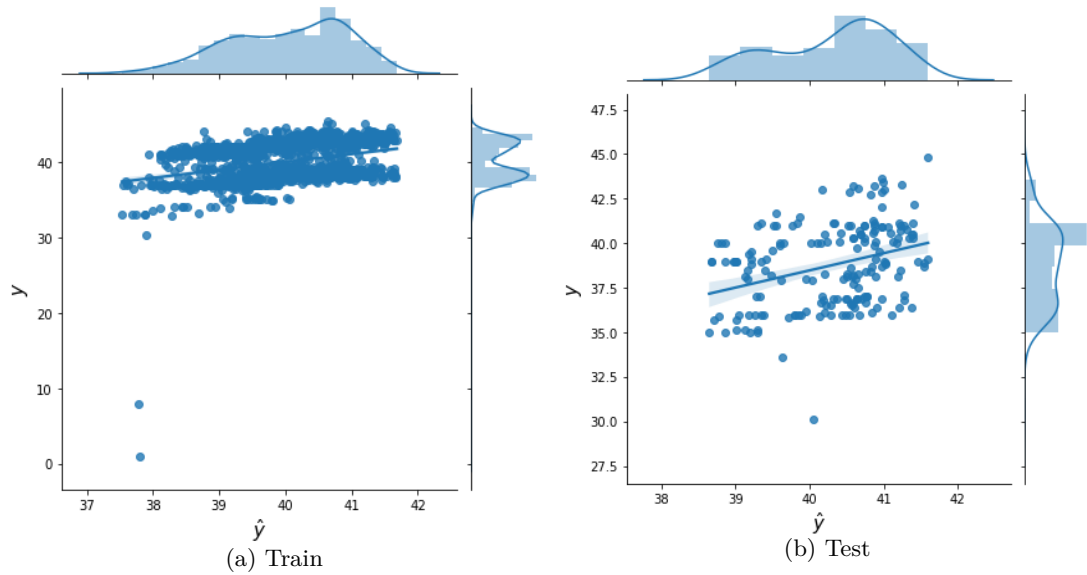


Figure 5.11: Learnt components from univariate Prophet

Data and predictions joint distribution

If the joint distributions for the true values y and the predicted values \hat{y} are plotted, it can be seen how the outlier in the training set was not learnt and how the approximation becomes erratic in the test set. Nonetheless, they already show a considerable improvement from the baselines distributions.

Figure 5.12: Univariate Prophet joint distributions of y and \hat{y}

5.2.4 Prophet implementation using exogenous regressors

To fully exploit the flexibility of GAMs, prophet's API allows defining custom regressors, which in the current work will be called exogenous variables as a resemblance of SARIMAX models. These variables are the ones explained in Chapter 2.

The overall performance can be seen in Figure 5.13. Compared to the univariate model, it can be seen that the confidence bounds now are narrower since there are less uncertainty in the predictions. It also can be seen that the model now is able to predict the trend change in the test set.

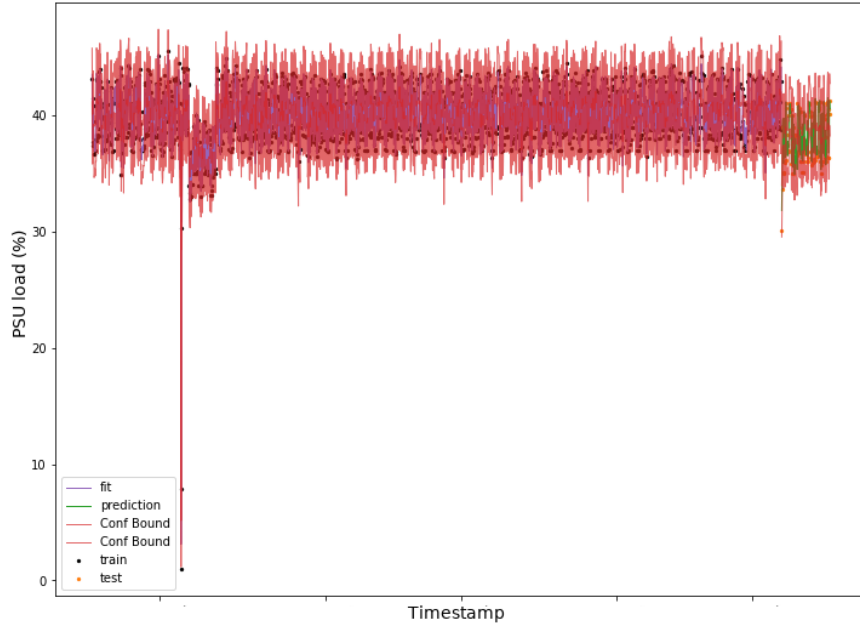


Figure 5.13: Training, test and predictions from multivariate Prophet

5.2.4.1 Model learnt components

The model components now show the additive factor of all the exogenous regressors, which seems to contain the information not learnt by the univariate training residuals.

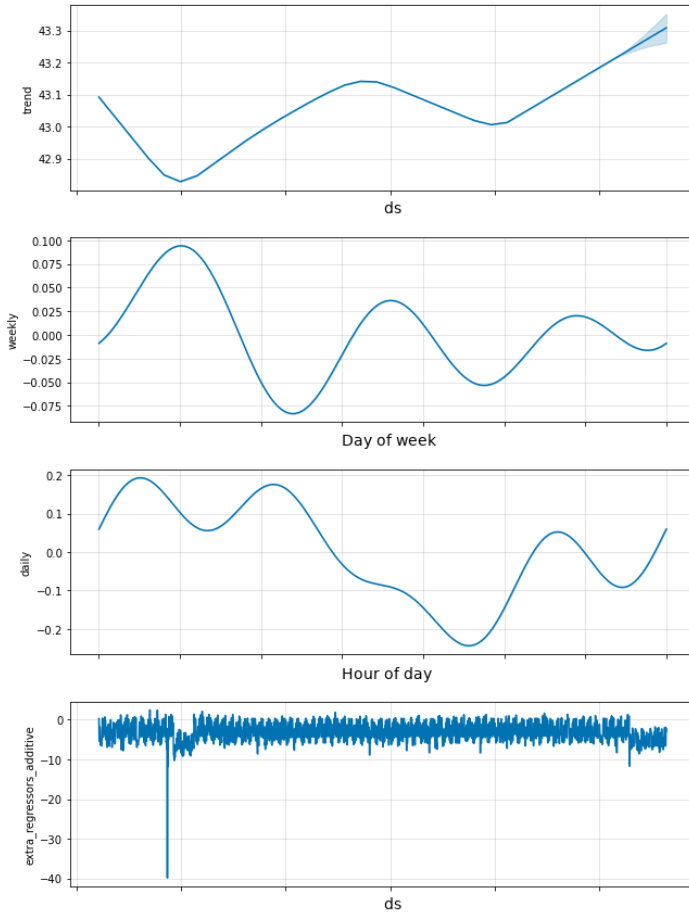
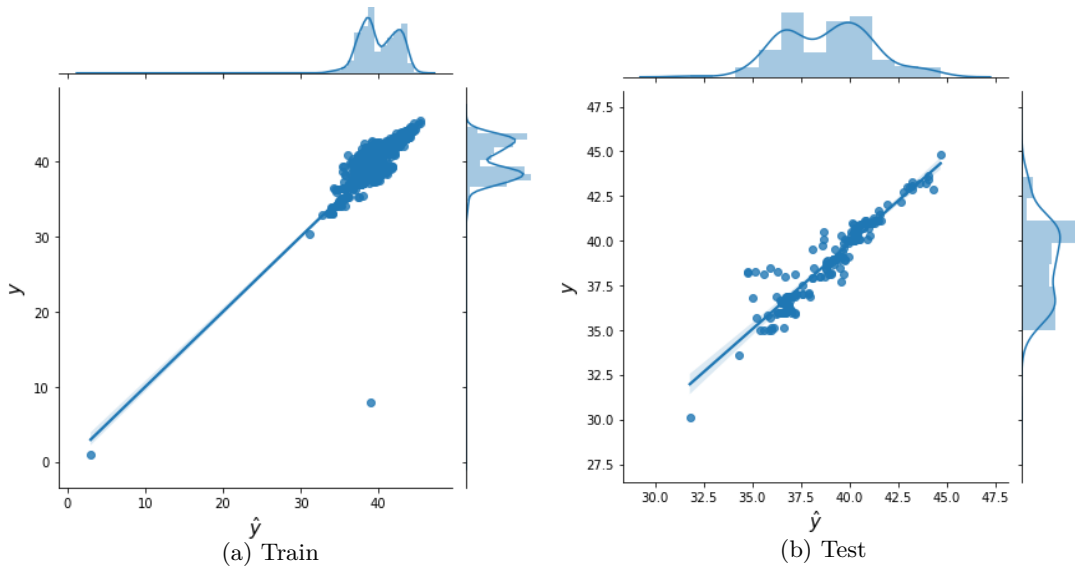


Figure 5.14: Learnt components from multivariate Prophet

Data and predictions joint distribution

The joint distributions for y and \hat{y} in Figure 5.15b now shows that the model has a significant improvement in its predictions accuracy compared against the baselines.

In the plot for the training set, it can be seen that the trend model detects the change without over-fitting which is confirmed in the testing set where the results show that the process has been well approximated due to the positive trend in the correlation between y and \hat{y} despite there is a trend change in the testing dataset.

Figure 5.15: Multivariate Prophet joint distributions of y and \hat{y}

5.2.5 Example forecast performance comparison

In order to quantify the long-range predictions improvement done by the usage of Prophet, in Table 5.2 their performance scores are summarised.

	MAE	R^2	MOBE	RMSE
Univar - Train	2.16	0.14	0.04	2.53
Univar - Test	2.11	-0.57	0.04	2.70
Multivar - Train	0.55	0.83	0.05	1.13
Multivar - Test	0.57	0.85	0.03	0.85

Table 5.2: Prophet's long-range prediction performance example

In this example, it can be observed the significant improvement done by the use of the exogenous predictors in the multivariate model, obtaining a $R^2 = 0.85$, which for a non-linear case can be considered a good approximation.

5.3 Exhaustive forecasting experiments

After being able to visualise how the models comparatively perform for an example case, it is needed to obtain a general view of how they perform. Therefore, similar to the experiments in Section 5.1, it is performed an exhaustive iterative evaluation of the predictions while moving the predicting horizon further and further.

In the following subsections, the exhaustive baseline results are presented and then Prophet's results are obtained to visualise its general improvement.

5.3.1 Baselines predictions moving horizon

Figure 5.16 shows overlapped the Auto-ARIMA and structural model performances. The curves are interesting due to their peak-valley seasonal-alike shapes. Their possible explanation is related to the original signal peaks and valleys variability, i.e., the minima are more show less variability than the maxima. Therefore, the predictions for the minima are less error-prone than for the maxima.

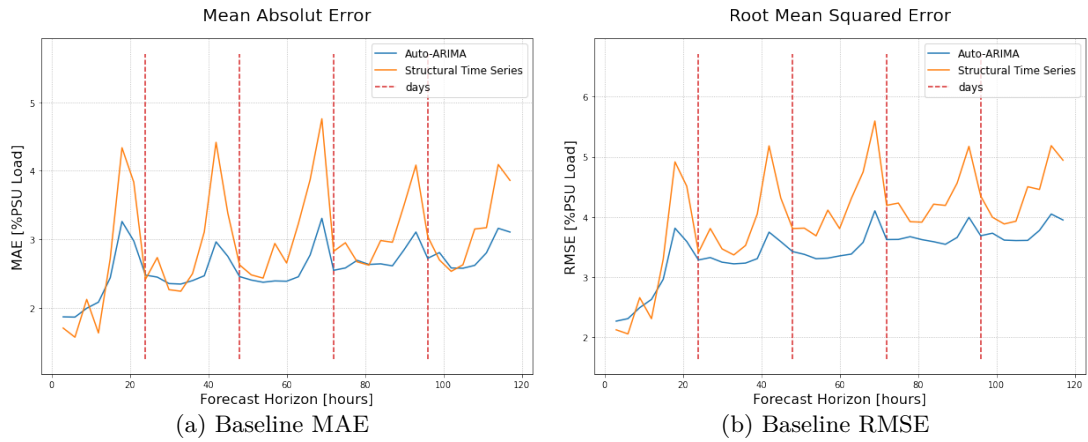


Figure 5.16: Baseline predictions performance vs forecast horizon time

On the other hand, it can be seen than opposed to the results for the imputation phase, the structural model provides poorer predictions than the ARIMA. Thus, if any of the baselines would have to be chosen, the Auto-ARIMA would be the best candidate.

5.3.2 Univariate Prophet prediction moving horizon

This set of experiments have been found requiring great computing power and time. Since the following overall experiment took ~ 17 hours to finish, it has been limited to sampling 50 models performances for a 3 days long-range horizon maximum.

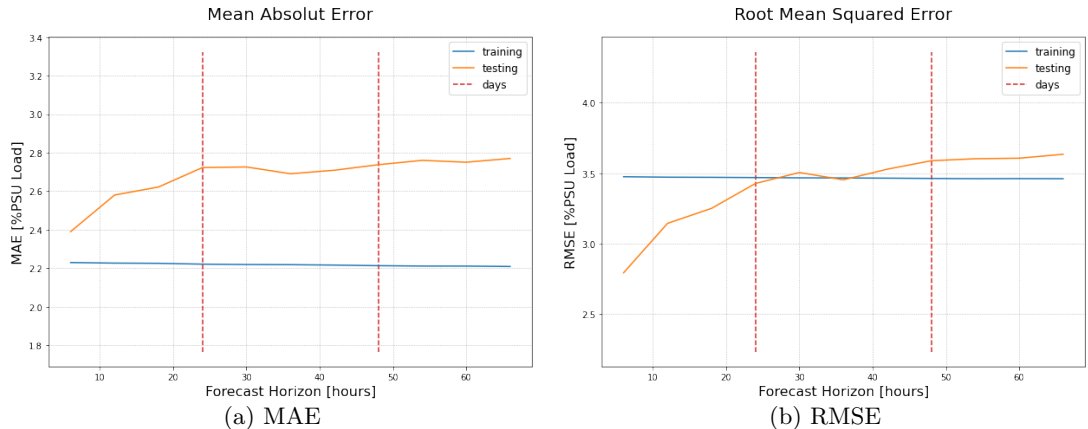


Figure 5.17: Univariate Prophet predictions performance vs forecast horizon time

In the results in Figure 5.17, it can be observed that as long the time horizon increases, as expected, the prediction errors tend to increase also. While MAE show that the prediction errors are consistently higher than the training error, the RMSE shows lower scores for the testing set than for the training when the time horizon is close to the present time. This inflection can be explained by the fact that RMSE penalises higher the large errors compared to MAE.

It is important to notice that, as the PSU utilisation signal is already in per-cent, these results are easily interpretable as per-cent error also. Therefore, in the long-range, an univariate Prophet model, shows that in average it can achieve MAE ~ 2.5 and RMSE ~ 3.6 PSU per-cent utilisation.

5.3.3 Multivariate Prophet prediction moving horizon

Now it is the turn of a Prophet model with external regressors that, in the first example, showed the best performance, therefore, it is expected to maintain that tendency but now with more confidence that the performance in the example was not some fortunate random event.

These experiments have consumed even more computing time than the previous in Section 5.3.2 , having spent more than 18.5 hours to finish.

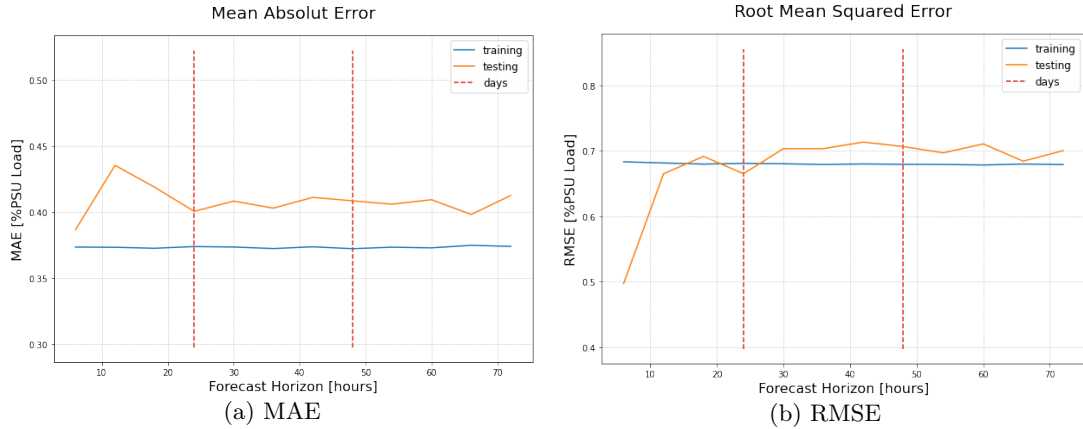


Figure 5.18: Multivariate Prophet predictions performance vs forecast horizon time

The results in Figure 5.18 show that the long-range prediction results for the Prophet model using exogenous regressors are consistently good having both, MAE and RMSE below 1%.

Other noticeable results are the ones shown in Figure 5.19, in which the R^2 scores in long-range are ~ 0.88 . Although it might seem unintuitive having better R^2 in the long range rather in the short term, it can be explained by the amount of data used to compute the score. The less data, the likely to have *a general bad approximation*.

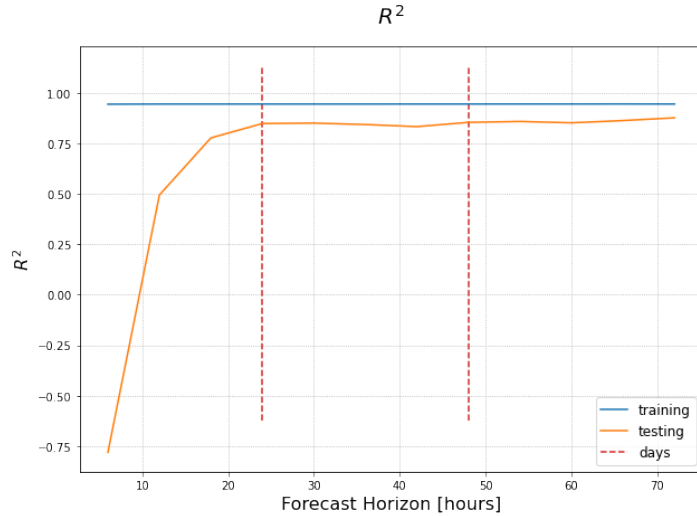


Figure 5.19: Multivariate Prophet R^2 vs forecast horizon time

5.3.4 Time performances

Figure 5.20 shows the average consumed time for running the exhaustive experiments in Ericsson's computing farm. It can be seen that the testing time is very similar for univariate and multivariate case. On the other hand, the training time for the multivariate model is slightly higher than the univariate one. Nonetheless both are under the half of second (average). It is also interesting that the longer the prediction range, the times remain almost constant.

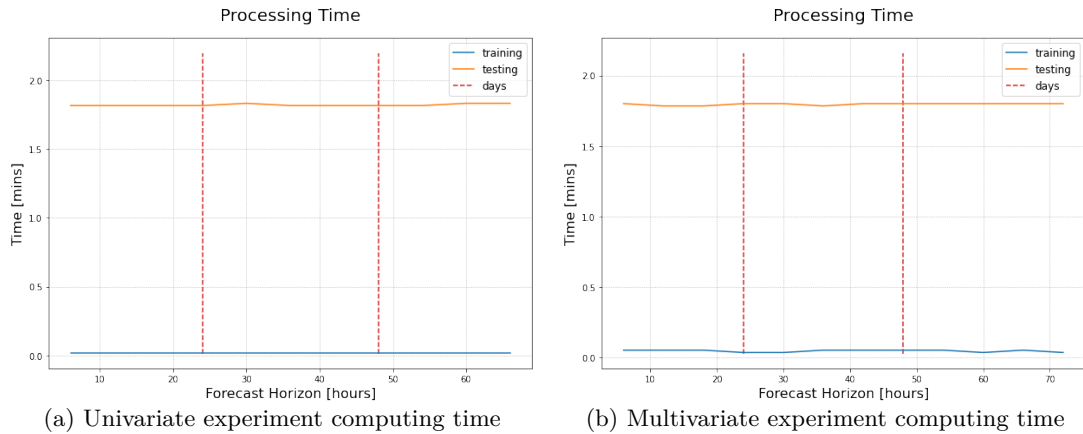


Figure 5.20: Experiments computing times

5.4 Performance summary

Finally, this section summarises the mean performances per day for all of the models under analysis for the ease of comparison.

Table 5.3 shows that the Prophet model with exogenous regressors vastly outperforms the other methods in terms of MAE.

Model	1 day	2 day	3 day
Structural	2.55	3.17	3.08
ARIMA	2.59	2.812	2.70
UniVar-Prophet	2.88	2.96	3.01
MultiVar-Prophet	0.41	0.40	0.40

Table 5.3: MAE Summary of models performance by day

Likewise, in Table 5.4, it can be observed the long-range stability of the multivariate Prophet model having, again, the best RMSE scores.

Model	1 day	2 day	3 day
Structural	3.27	4.31	4.35
ARIMA	3.22	3.77	3.81
UniVar-Prophet	3.54	3.88	4.02
MultiVar-Prophet	0.62	0.71	0.68

Table 5.4: RMSE Summary of models performance by day

Lastly, Table 5.5 presents how the multivariate Prophet model is even capable of having acceptable R^2 scores, which in this type of data is not an easy task.

Model	1 day	2 day	3 day
Structural	-7.23	-8.90	-2.90
ARIMA	-95.76	-2.25	-0.23
UniVar-Prophet	-203.76	-1.04	-0.98
MultiVar-Prophet	0.33	0.85	0.86

Table 5.5: R^2 Summary of models performance by day

5.5 Power headroom estimation

Until this point of the work, the research has been mainly focused on PSU loads forecasting. Nonetheless, as mentioned in the introductory context, the goal is to predict the power headroom defined in (1.1). But as there are no direct measurements of power headroom that can be learnt, it is needed to derive it from the power consumption.

Therefore, to provide a power headroom forecast, after estimating the future values of the loads' consumptions, it is needed a further step to translate that information into power headroom terms. The following sections will propose a way to manage to achieve it and discuss other aspects of its technical applicability.

5.5.1 Power headroom derivation as PSU utilisation complement

As it has been exposed in Section 2.2.1, the power load is a measure of *how many percentual power capacity it is being used at that time*. Thus, it is straightforward to claim that the percentual power headroom is its complement.

If the interest is to obtain a measurement in Watts units, the installed power capacity in the RBS, P_{max} , is needed to be known so that its proportion can be computed as follows.

$$P_h[\%] = 100 - P_L[\%]$$

Where $P_h[\%]$: Power headroom in percents (5.6)

and $P_L[\%]$: Power loads consumptions in percents

If the interest is to obtain a measurement in Watts units, it is needed to know the installed power capacity, P_{max} , in the RBS so that its proportion can be computed as showed in (5.7).

$$P_h = P_{max} \cdot \frac{P_h[\%]}{100}$$
(5.7)

Where P_{max} : Installed power capacity in Watts

In Figure 5.21, it is shown the PSU utilisation signal used as example test in Chapter 3.2 and its derived power headroom.

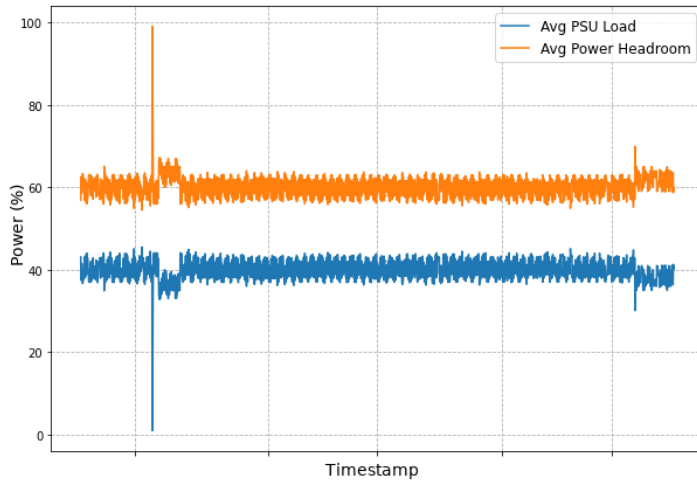


Figure 5.21: Power headroom derivation from PSU Load

5.5.2 Criterion considerations

In general terms, an alarm is meant to notice that something abnormal is happening in a process or, in a forecasting context, may (or will) occur in the future and support the operator response [47].

In the current works' context, the alarm meaning can be conceived as the RBS not having enough power to manage to keep its by-design behaving.

Although it should be possible to define how likely a power overload is given the system's current state in probability terms, triggering an alarm is a binary task. The system is operating either in a "*safe*" or in an "*abnormal*" region. Then crossing a boundary that separates these two regions is the trigger for the alarm.

There are different techniques to tune an optimal trigger level. It could be done based on a system variable, or a latent variable or even a joint distribution of the two kinds [48].

Choosing the best possible boundary is considered to be out of the current work scope. Nonetheless, as an initial approach, it can be proposed to be settable by the user according to their needs and expertise.

From this assumption and the derivations in (5.6) and (5.7), the following guidelines should be taking into consideration.

Values interpretation

Percentages values are not always able to fully represent the system conditions. For example, it is very different having 10% of power headroom where the total capacity is 10 kW and 1 kW since the relative oscillations could be drastically different. Therefore, the power magnitude should be taken into consideration.

PSUs do not partially fail

The power capacity is not continuous. It will have discrete values as shown in Figure 5.22, and also, the PSUs can have different power contributions. This means that in order to set the threshold is needed to take into account the worst-case scenario, which would be "*can the RBS work if the next failure is the most power contributing PSU*".

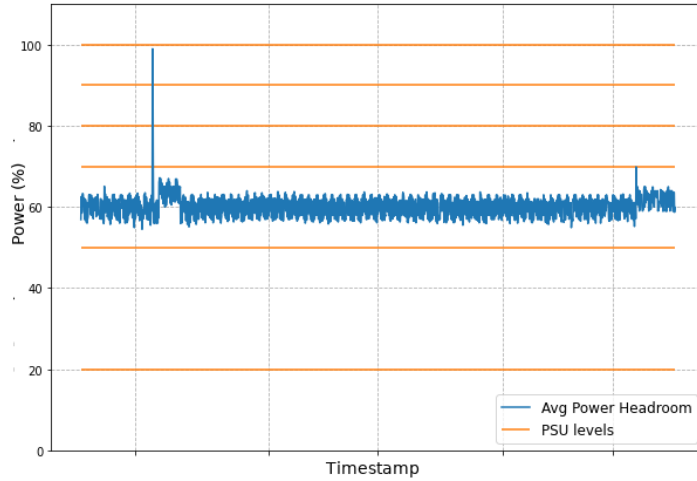


Figure 5.22: Power headroom and discrete availability in percents

5.5.3 Alarm triggering and the n -level safety criteria

Let P_{max} be the maximum power capacity installed and working in an RBS, \bar{P}_{Load} the average PSU utilisation and Δp the confidence interval used when training the Prophet model. Let N be the amount of working PSUs, let $\{P_{PSU_1}, \dots, P_{PSU_N}\}$ such that $P_{PSU_1} > \dots > P_{PSU_N}$ are the descending sorted power contributions from the working PSUs.

Then, let the n -level safety criteria, be the n amount of worst-case PSU failures to keep as operational margin:

$$\begin{aligned} P_{max} - \sum_{i=1}^n P_{PSU_i} &> \bar{P}_{Load} + \Delta p \\ P_{max} - \{\bar{P}_{Load} + \Delta p\} &> \sum_{i=1}^n P_{PSU_i} \end{aligned} \quad (5.8)$$

But, as the power headroom is by definition the difference between the installed power capacity and the power being consumed.

$$\begin{aligned} P_h &= P_{max} - \{\bar{P}_{Load} + \Delta p\} \\ P_h &> \sum_{i=1}^n P_{PSU_i} \\ \therefore P_{crit_n} &= \sum_{i=1}^n P_{PSU_i} \end{aligned} \quad (5.9)$$

Where P_{crit_n} is the n -level criteria threshold. Thus, whenever the power headroom forecast \hat{P}_h at time $t+k$, being t the current time, meets the condition in (5.10) a fault alarm must be triggered

$$\hat{P}_{h_{t+k}} \geq P_{crit_n} \quad (5.10)$$

6 Discussion

6.1 Results

After analysing the results from the imputation experiments and the prediction generalisation, it has been chosen structural time series models and multivariate Prophet for each stages respectively. In the Figure 6.1 it is shown how the pipeline has been defined.

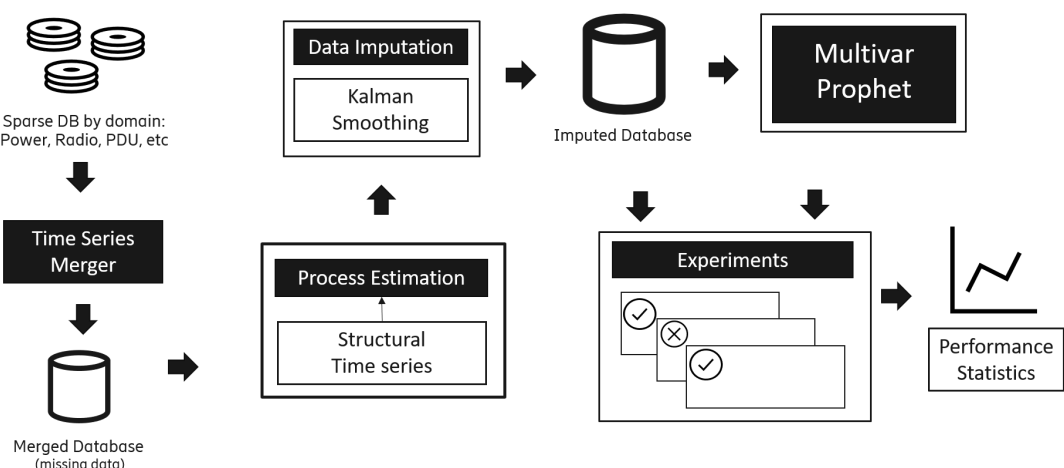


Figure 6.1: Final pipeline architecture

In the imputation stage, the Auto-ARIMA model has showed to be unstable for some features of the dataset, whereas the structural models have not. This, although, should not be understood as a failure of the SARIMA approach, yet an inconsistency of the auto-ARIMA algorithm not being able to reach a proper model through its heuristics that, even though it has been published and implemented in a popular library, still have some arbitrary steps.

When it comes to compare the baselines performances against the univariate Prophet model, it can be seen that the latter sometimes performs even worse than the baselines, which might induce some critical thoughts about Prophet as a good framework. Nonetheless, when adding exogenous regressors is when the model shows its power by lowering significantly the

error rates, and even more being able to reach $R^2 > 0.8$ values, which can be considered a good approximation given the nature of the target signal.

Even though it has been presented a derivation of the power headroom from the PSU utilisation. The n -level criteria has not been tested in a case that meets the criteria and trigger an alarm.

6.2 Methods

6.2.1 Time series merging

In the current case, to build the database, it has been decided to merge the time series with an outer join and then impute the missing data rather than using inner joins and a reduced amount of data. Nevertheless, this does not mean that this approach is always the recommended approach. A further study that could have been done is to extract the *longest* uncorrupted piece of time series $\{\mathbf{U}_t\} \subseteq \{\mathbf{Y}_t\}$ and run statistical tests to measure their similarities and determine if subseries $\{\mathbf{U}_t\}$ is *representative* of the complete series $\{\mathbf{Y}_t\}$.

This scenario could happen when having a very long time series in highly seasonal data, which, unfortunately, it was not the case for the available data since extrapolating two months to an entire year might be risky in a real communications application.

6.2.2 Time series imputation

It has been only used univariate approaches to estimate the model and smoothen the signals, which implicitly –and naively– implies that the features are independent and no correlations can be found between them. This decision was intentionally made to set a baseline and, as the first attempt on this domain within the company, prioritising simplicity over sophistication.

It should be noted that multivariate imputing techniques could improve the processing time and the accuracy of the imputation.

6.2.3 Forecast

The Prophet model was chosen as a predictive model mainly for its novelty, flexibility, and well-proven usage in the social networks industry. Besides its theoretical attractiveness, it is also well suited for time-limited work due to its well-designed API and available documentation. Nonetheless, this means that apart from scientific curiosity and pragmatic planning, there are no strong arguments to state that it is the best-suited model.

Other than Prophet, it was explored a boosted decision trees regressor using XGBoost, which showed promising results. Nonetheless, its current implementation status can be considered half-done and, therefore, its results cannot be conclusive.

It has also been noticed that the time series models estimated by Auto-ARIMA and structural time series to perform the imputing phase can be reused to forecast. Although it seems straightforward mathematically, from an implementation perspective, it is not. As mentioned in Section 6.2.2, the imputing has been done naively from a univariate approach. Thus, the forecasting model would only learn from the average power load. Nonetheless, for future developments in which a multivariate imputing strategy is taken, it is undoubtedly an alternative that must be considered.

There is also an implementation complexity related to it. The model estimation and imputing stages have been implemented using R, whereas the rest of the work has been done in Python. In order to make both languages interact it has been used rpy2 package nonetheless, it has also made the code more intricate and increased the development time.

6.3 Ethical considerations

The project aims to open a research line towards the decreasing of telecom operator companies operational costs. Nonetheless, this is not limited to a purely economic benefit to the companies. Maintenance duties can imply some risks to the field workforce when, for instance, the RBS is located in a remote location. Therefore, this project effects will be also beneficial for the field personnel.

Environmentally wise, reducing the number of trips and interventions in remote locations, which could be close to nature wildlife, will also contribute to reduce the pollution levels related to them and invade less the wildlife space.

Although the project's domain is in mobile communications, it is directly related to human behaviours. Therefore, analysing how this may be affected by social biases and whether its effects could be more beneficial towards one group of people or detrimental to others is, in fact, a moral obligation from the researcher's and developer's perspective.

In that line, it is crucial to state that different groups of people behave differently. Therefore, the seasonalities learnt from data from one country may not reflect the customs in others, especially when it is related to holidays or temperature. As a consequence, it can be stated that when a system of this nature is deployed to service, it needs to learn from data coming from the region where it is being deployed or some other statistically similar.



7 Conclusion

It has been explored and evaluated different techniques to manage univariate time series from sparse file sources and synchronise them in just one multivariate time series data structure. For this case, if they would be merged using an outer join approach, it would affect the length of the series since only the intersections would be included, and even more, if there was any missing sample, it could violate the constant sampling time assumption. Hence, using an inner join approach was more reasonable.

Nonetheless, by using an inner join to merge the time series, NaN values were introduced, making prophet fail. Consequently, it was decided to impute them by using Kalman smoothing from model approximations obtained from structural time series estimation by maximum likelihood or a SARIMA auto fitting using the algorithm in [43]. It was observed that when simulating MCAR from complete data and then comparing the estimates, structural time series modelling tends to approximate better and behave more stable than auto-ARIMA models.

Since the only forecasting model with conclusive results has been prophet, there is no solid fundament for concluding that it is, in fact, the most suitable model for this application. Nonetheless, it still shows the ability to accurately estimate the power consumption ranges not being largely affected by changes in the trend or outliers.

It has been analytically derived how to compute in real-time the power headroom and, considering that the power reductions are not continuous but quantised, it has been concluded that the power headroom cannot be less than the largest PSU power contribution. Furthermore, this conclusion has been extended, and an n -level safety criterion has been proposed.



8 Future work

Imputing the data was not initially considered as part of the project. However, after running into issues with Prophet due to NaN values, it had to be decided between two options. First, the prediction model could have been changed for another that could handle missing data, or on the other hand, the merged time series could have been processed to fill the gaps so prophet would not fail. The latter was chosen, leaving the former unexplored due to time constraints. Future works could research in that direction and evaluate how much improvement is obtained from imputing the data and conclude whether this choice was correct or not.

It will also be interesting to research multivariate time series imputation techniques and replace the several independent univariate imputations done in this work, getting rid of the naive -and known wrong- assumption of independence between the features. In the same stage, the processes estimations should not be discarded since they can be reused to forecast power consumptions.

Further research must be done exploring other alternatives, such as the mentioned XGBoost regressor with promising inconclusive results or Recurrent Neural Networks or Transformers, to mention some others.

The proposed alarm criteria have been analytically derived. Although it works to set a reasonable threshold, it still relies on an expert to tune its value. In order to fully automate the new predictive alarm system, it is also needed to apply an optimisation technique to find the best alarm criterion. When it comes to evaluating an eventual deployment of the service, the current approach needs to collect some time of data from the actual RBSs since it has been conceived as *ad hoc* solutions, which might not be the ideal solution at all.

The initial conceptualisation of this work was to train a faults predictor, so the installed power capacity was the most critical variable to predict. Unfortunately, after mining more than a thousand RBSs data, only six faults suspicions were found, forcing the change of the approach to a power demand forecasting and assuming the power capacity as a constant. The final solution must get rid of this assumption and change the P_{max} value to another forecast $P_{max}(t)$ being evaluated by faults predictors.

During the research, it has been noted that, in appearance, there is no unique pattern preceding a PSU fault. Thus, if the final goal is to pre-train some models to be deployed without collecting data on-site, these suspected failure modes should be studied. It has been proposed to cluster the faults and investigate the possibilities to treat them as they were the same RBS.

A

Further results

A.1 Baseline predictions

A.1.1 Structural time series

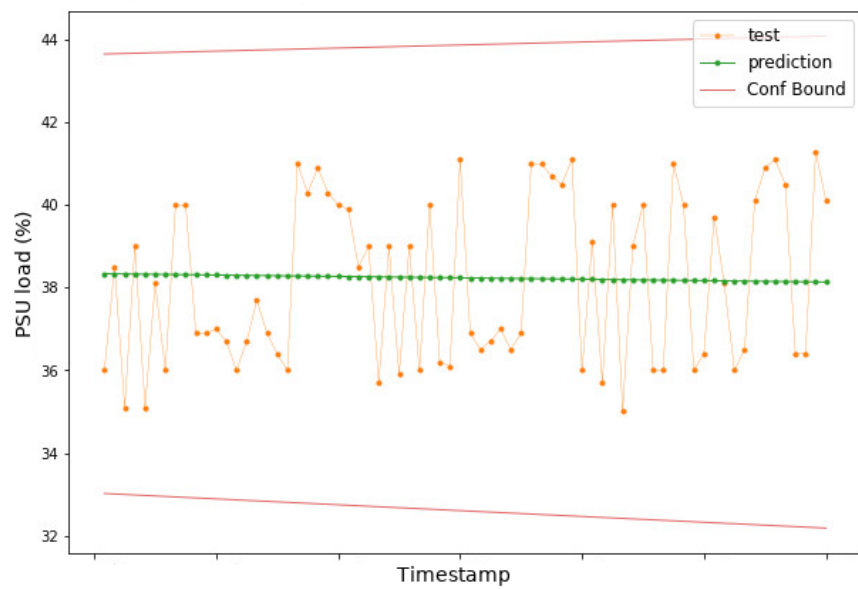


Figure A.1: Structural model 3-days baseline predictions

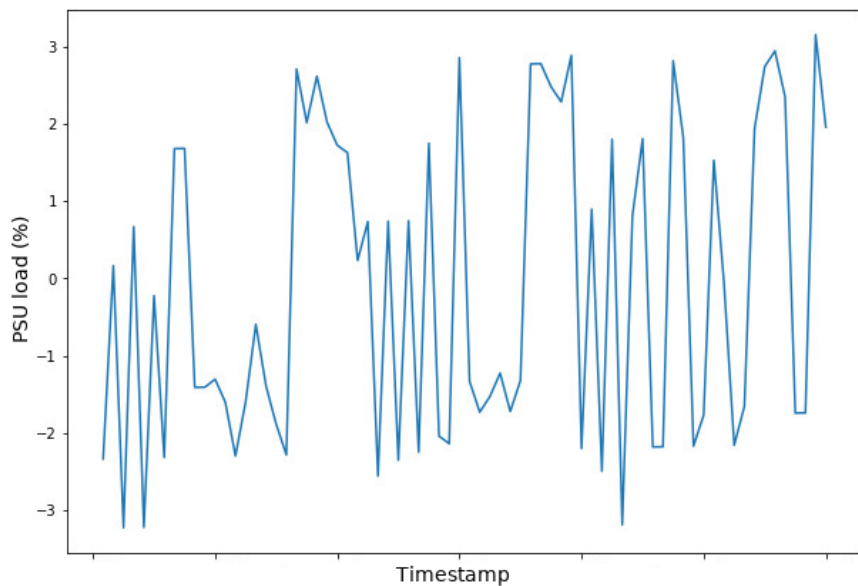


Figure A.2: Structural model 3-days baseline residuals

A.1.2 Auto-ARIMA

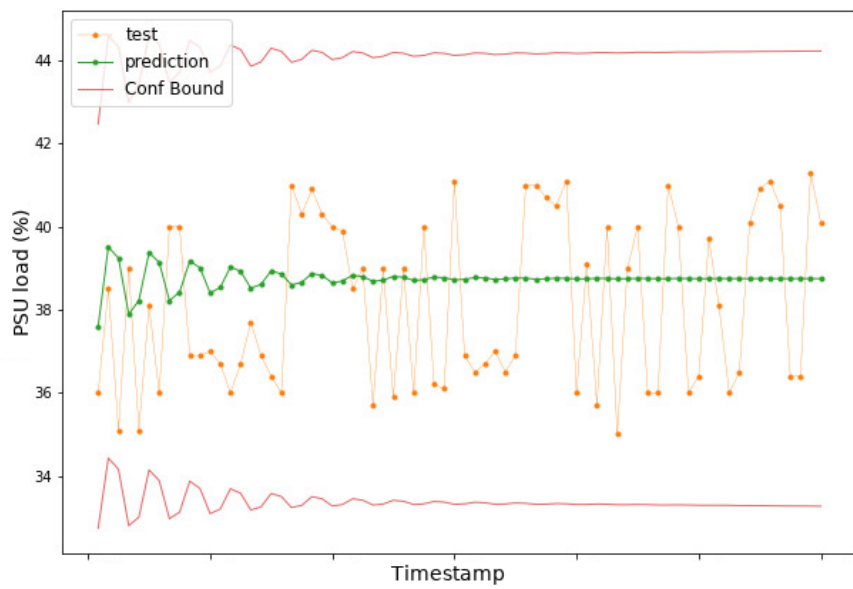


Figure A.3: Auto-ARIMA 3-days baseline predictions

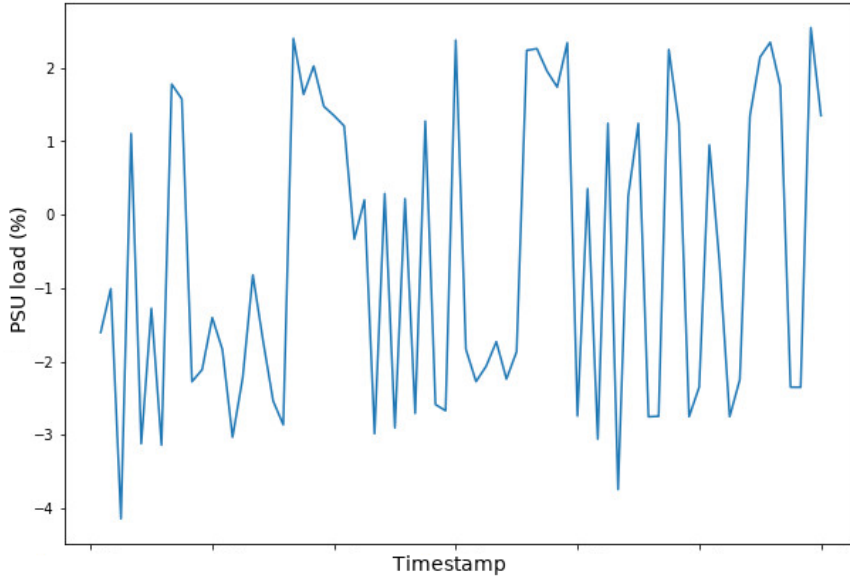


Figure A.4: Auto-ARIMA 3-days baseline residuals

A.2 Univariate Prophet

A.2.1 Training fitting

In training is obtained a very poor R^2 value, which from the plot in figure A.5 can be expected, since \hat{y} looks like mostly an average of the seasonal components. Nonetheless, if it is considered that predicting an interval is acceptable, then the MOBE shows a very good result.

It can also be observed that the trend component did not overfit to the outliers.

MAE	2.20
R^2	0.11
MOBE	0.08

Table A.1: Univariate prophet training scores

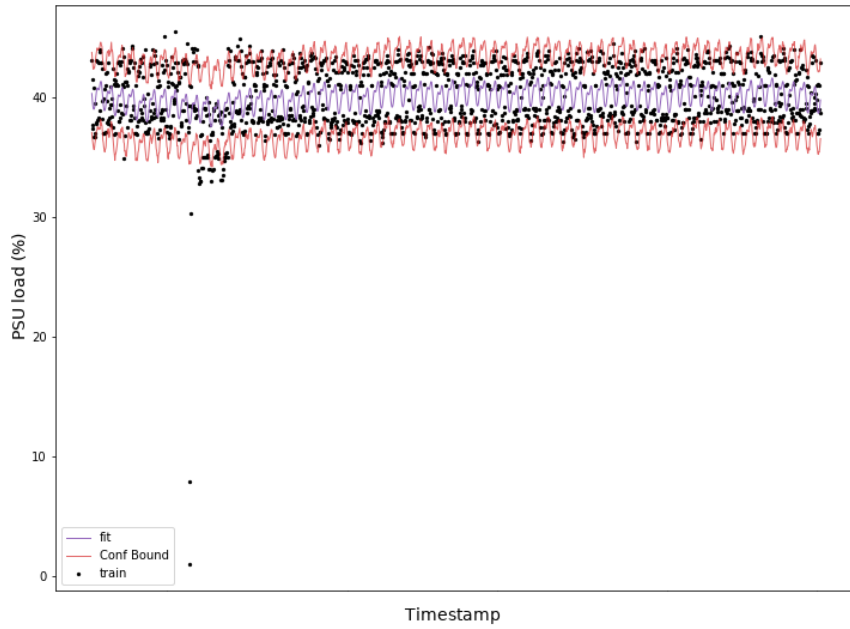


Figure A.5: Training fitting from univariate prophet

A.2.2 Test predictions

When it comes to the predictions performance, the R^2 shows even worse results. The MOBE is also high since the trend component was not able to foresee the decreasing in the middle of the test set as shown in Figure A.6.

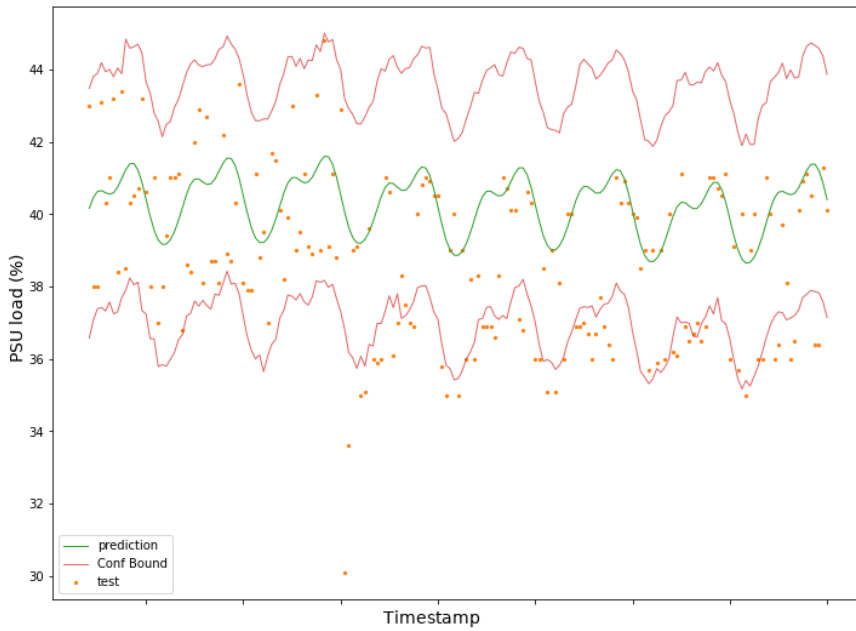


Figure A.6: Test predictions from univariate Prophet

MAE	2.12
R^2	-0.33
MOBE	0.25

Table A.2: Univariate prophet prediction performance

A.2.3 Residual analysis

The residuals in the training set still show somehow resembles the original data pattern. This could be interpreted that there is still patterns to learn from data, i.e., this model is not complete.

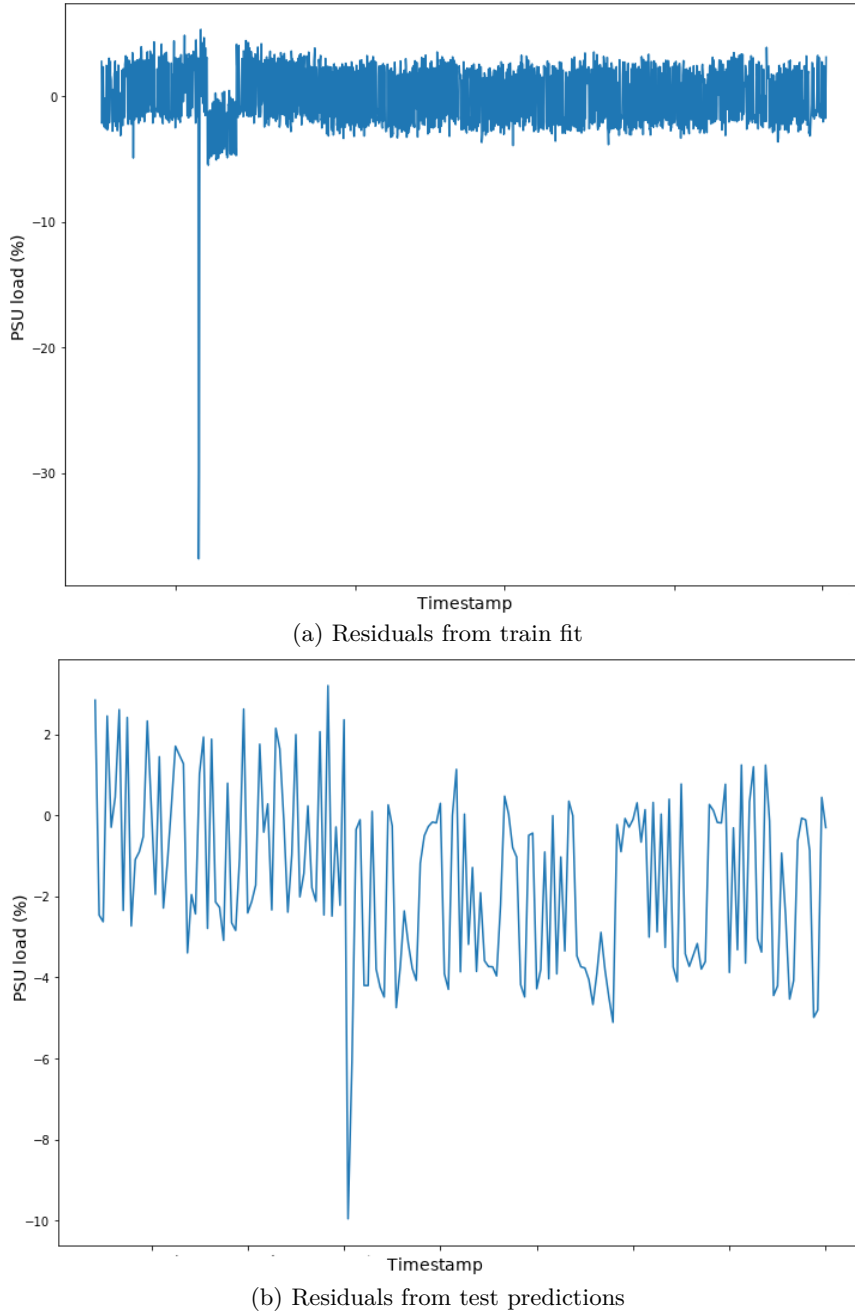


Figure A.7: Univariate prophet residuals

A.3 Multivariate Prophet

A.3.1 Test predictions

The results of the predictions have notoriously improved in this case. The R^2 value is close to 0.9, which for such a complex signal shows how powerful is the model.

The MOBE has even decreased in the test set, this could be due to training outliers that still being difficult to approximate without overfitting the trend component.

MAE	0.52
R^2	0.88
MOBE	0.05

Table A.3: Multivariate prophet prediction performance

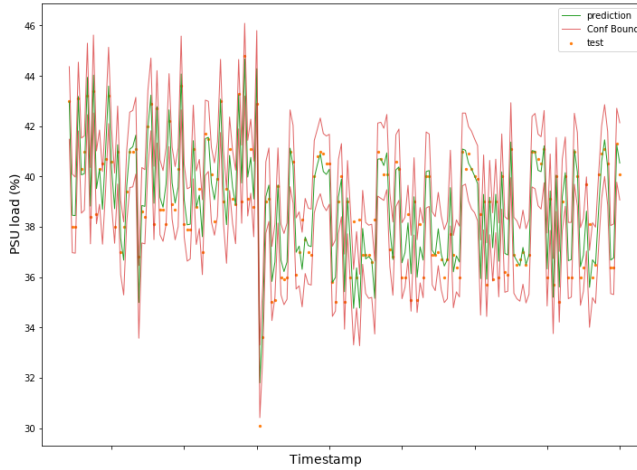


Figure A.8: Test predictions from multivariate prophet

A.3.2 Residual analysis

The residuals show that the patterns have been better learnt than in the univariate case.

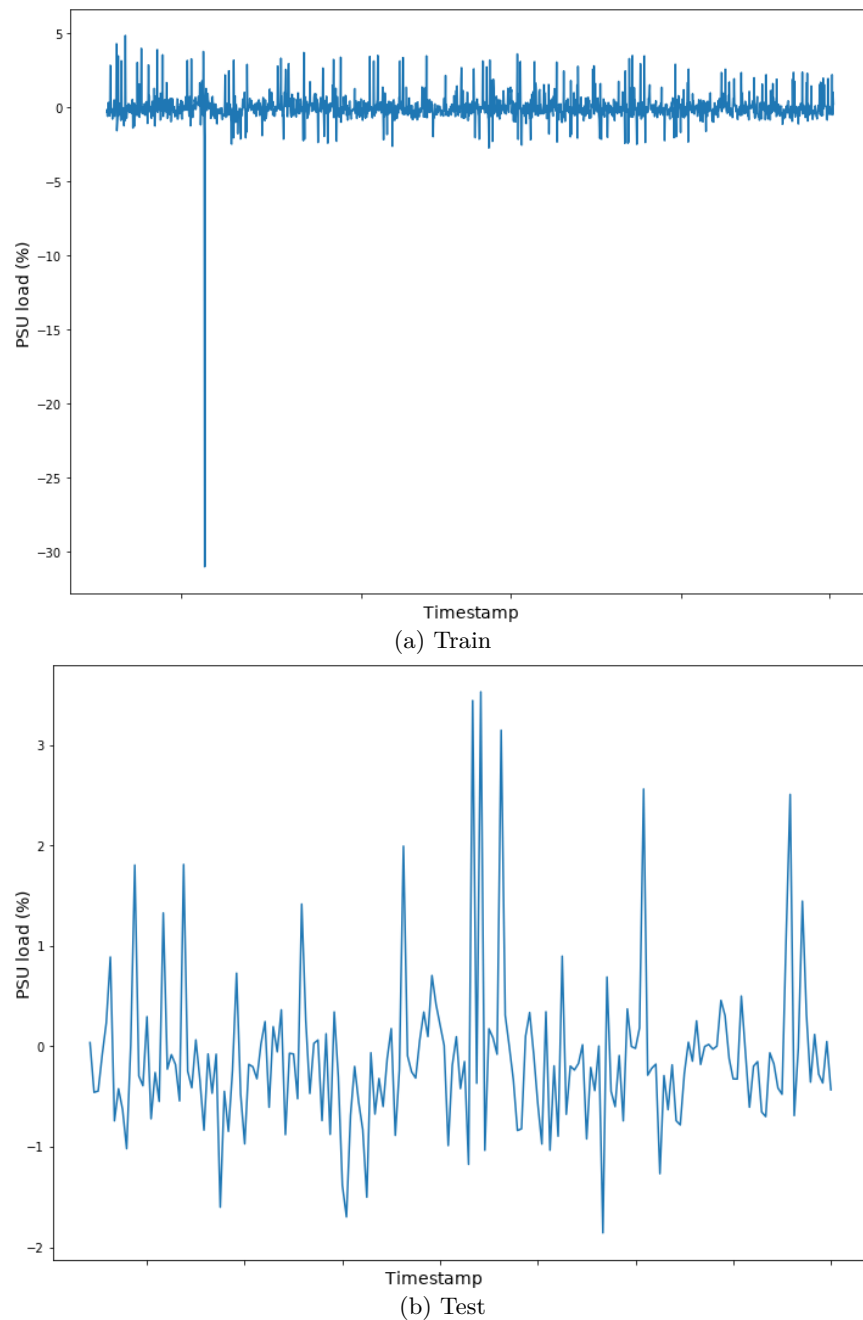


Figure A.9: Multivariate prophet residuals

A.4 Exhaustive experiments

A.4.1 Baselines predictions moving horizon

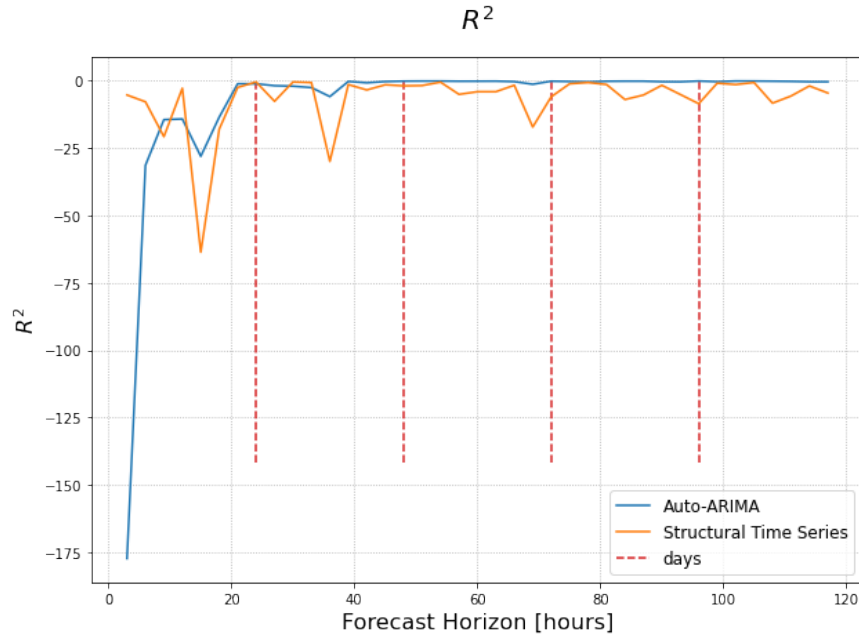
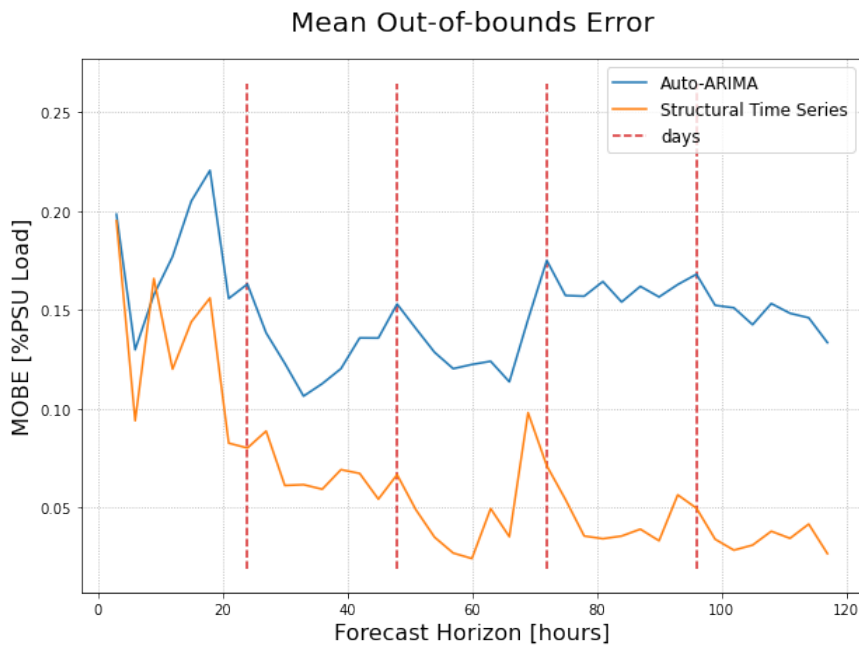
Figure A.10: Baseline R^2 

Figure A.11: Baseline MOBE

A.4.2 Univariate Prophet prediction moving horizon

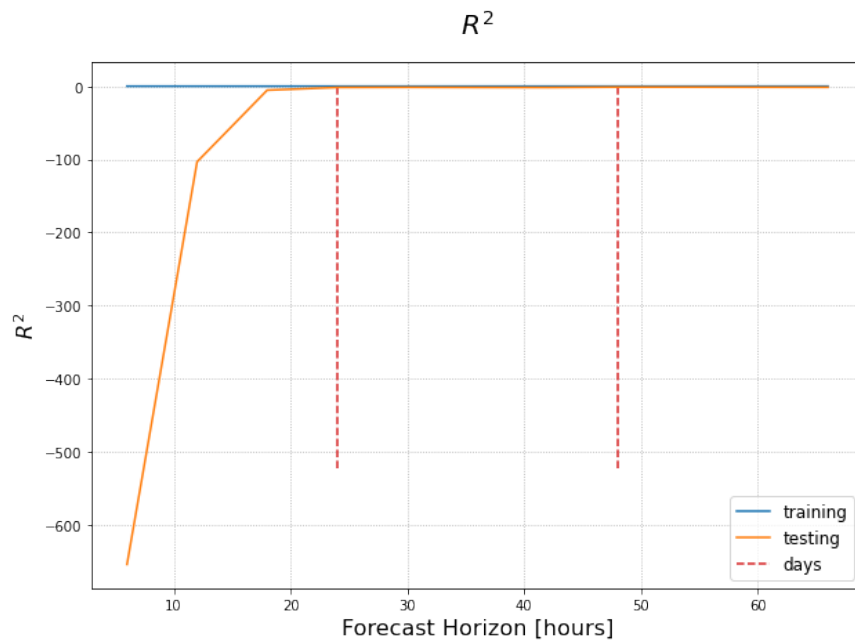
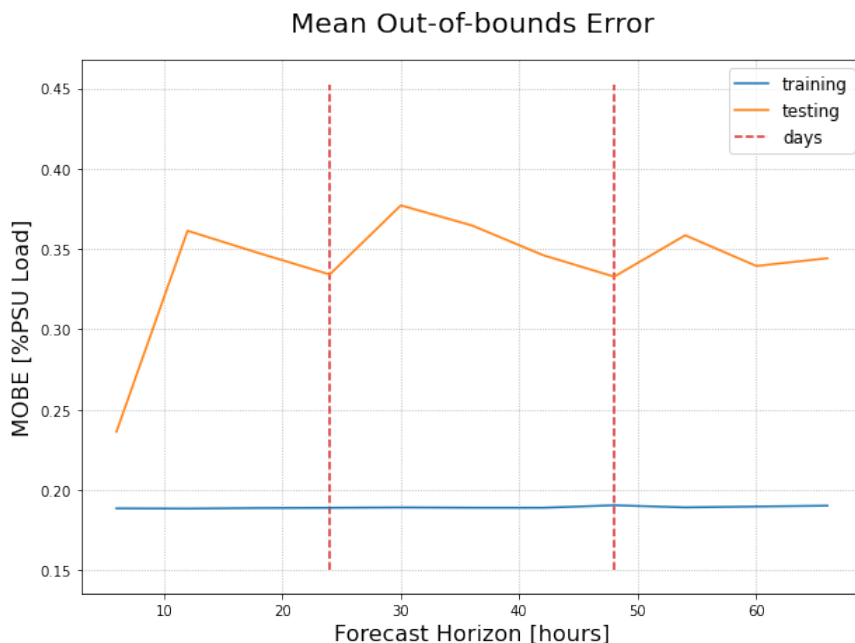
Figure A.12: Univariate moving prediction horizon: R^2 

Figure A.13: Univariate moving prediction horizon: MOBE

A.4.3 Multivariate Prophet prediction moving horizon

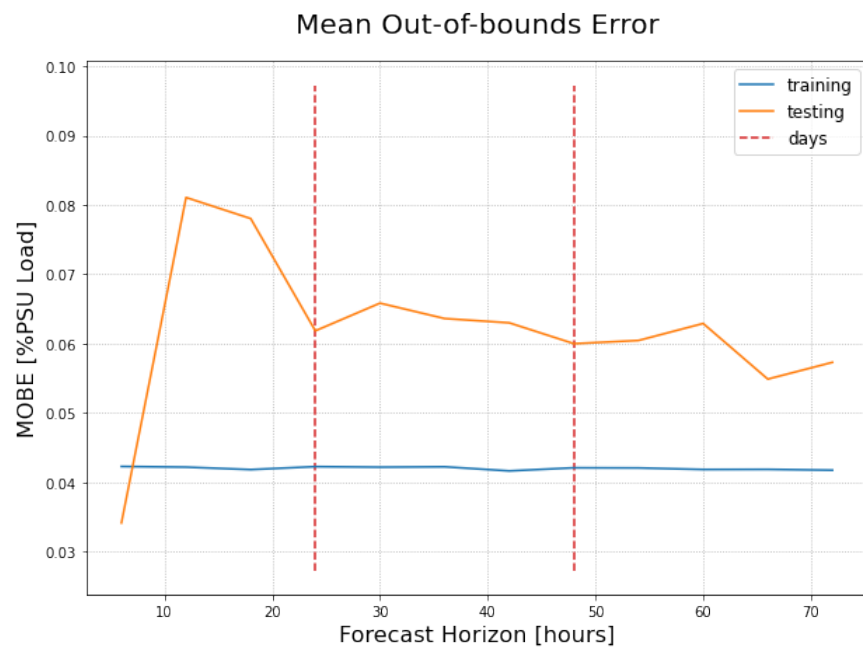
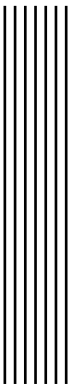


Figure A.14: Multivariate moving prediction horizon: MOBE



Bibliography

- [1] Bilal Muhammad and Abbas Mohammed. "Uplink closed loop power control for LTE system." In: *2010 6th international conference on emerging technologies (ICET)*. IEEE. 2010, pp. 88–93.
- [2] E-UTRA Physical Layer Procedures. "3GPP TS 36.213." In: *V11. 0.0, Sep* (2012).
- [3] Oliver Arnold, Fred Richter, Gerhard Fettweis, and Oliver Blume. "Power consumption modeling of different base station types in heterogeneous cellular networks." In: *2010 Future Network & Mobile Summit*. IEEE. 2010, pp. 1–8.
- [4] Bjorn Debaillie, Claude Dessel, and Filip Louagie. "A flexible and future-proof power model for cellular base stations." In: *2015 IEEE 81st Vehicular Technology Conference (VTC Spring)*. IEEE. 2015, pp. 1–7.
- [5] Alexandra Mourato, David Duarte, Iola Pinto, and Pedro Vieira. "A novel and realistic power consumption model for multi-technology radio networks." In: *URSI Radio Science Bulletin* 2018.364 (2018), pp. 20–29.
- [6] Peter R Winters. "Forecasting sales by exponentially weighted moving averages." In: *Management science* 6.3 (1960), pp. 324–342.
- [7] Pierpaolo Piunti, Simone Morosi, and Enrico Del Re. "Traffic Forecast and Power Consumption Management in Cellular Networks." In: *Traffic* 40.60 (), p. 80.
- [8] Mounir Achir and Laurent Ouvry. "Power consumption prediction in wireless sensor networks." In: *Proceedings of the 16th ITC Specialist Seminar on Performance Evaluation of Wireless and Mobile Systems*. Citeseer. 2004.
- [9] T Deepika and P Prakash. "Power consumption prediction in cloud data center using machine learning." In: *Int J Electr Comput Eng (IJECE)* 10.2 (2020), pp. 1524–1532.
- [10] DV Antonenkov and DB Solovev. "Mathematic simulation of mining company's power demand forecast (by example of "Neryungri" coal strip mine)." In: *IOP Conference Series: Earth and Environmental Science*. Vol. 87. 3. IOP Publishing. 2017, p. 032003.
- [11] Jingxiang Lv, Tao Peng, Yingfeng Zhang, and Yuchang Wang. "A novel method to forecast energy consumption of selective laser melting processes." In: *International Journal of Production Research* (2020), pp. 1–17.

- [12] Abdulwahed Salam and Abdelaaziz El Hibaoui. "Comparison of Machine Learning Algorithms for the Power Consumption Prediction : - Case Study of Tetouan city –." In: *2018 6th International Renewable and Sustainable Energy Conference (IRSEC)*. 2018, pp. 1–5. DOI: [10.1109/IRSEC.2018.8703007](https://doi.org/10.1109/IRSEC.2018.8703007).
- [13] Yao Cheng, Chang Xu, Daisuke Mashima, Vrizlynn LL Thing, and Yongdong Wu. "PowerLSTM: power demand forecasting using long short-term memory neural network." In: *International Conference on Advanced Data Mining and Applications*. Springer. 2017, pp. 727–740.
- [14] Songpu Ai, Antorweep Chakravorty, and Chunming Rong. "Household power demand prediction using evolutionary ensemble neural network pool with multiple network structures." In: *Sensors* 19.3 (2019), p. 721.
- [15] Abdulla I Almazrouee, Abdullah M Almeshal, Abdulrahman S Almutairi, Mohammad R Alenezi, and Saleh N Alhajeri. "Long-Term Forecasting of Electrical Loads in Kuwait Using Prophet and Holt–Winters Models." In: *Applied Sciences* 10.16 (2020), p. 5627.
- [16] RJ Chadalavada, S Raghavendra, and V Rekha. "Electricity requirement prediction using time series and Facebook's PROPHET." In: *Indian Journal of Science and Technology* 13.47 (2020), pp. 4631–4645.
- [17] Yuan jiang Li, Yi Yang, Kai Zhu, and Jinglin Zhang. "Clothing Sale Forecasting by a Composite GRU-Prophet Model With an Attention Mechanism." In: *IEEE Transactions on Industrial Informatics* (2021).
- [18] Donald B. Rubin. "Multiple Imputation after 18+ Years." In: *Journal of the American Statistical Association* 91.434 (1996), pp. 473–489. DOI: [10.1080/01621459.1996.10476908](https://doi.org/10.1080/01621459.1996.10476908).
- [19] Arthur P Dempster, Nan M Laird, and Donald B Rubin. "Maximum likelihood from incomplete data via the EM algorithm." In: *Journal of the Royal Statistical Society: Series B (Methodological)* 39.1 (1977), pp. 1–22.
- [20] PM Vacek and T Ashikaga. "An examination of the nearest neighbor rule for imputing missing values." In: *Proc. Statist. Computing Sect., Amer. Statist. Ass* (1980), pp. 326–331.
- [21] Barry L Ford. *An Overview of Hot-Deck Procedures: Incomplete Data in Sample Surveys*, Vol. 2. 1983.
- [22] Steffen Moritz, Alexis Sardá, Thomas Bartz-Beielstein, Martin Zaefllerer, and Jörg Stork. "Comparison of different Methods for Univariate Time Series Imputation in R." In: *arXiv e-prints*, arXiv:1510.03924 (Oct. 2015), arXiv:1510.03924. arXiv: [1510.03924](https://arxiv.org/abs/1510.03924).
- [23] Steffen Moritz and Thomas Bartz-Beielstein. "imputeTS: Time Series Missing Value Imputation in R." In: *The R Journal* 9.1 (2017), pp. 207–218. DOI: [10.32614/RJ-2017-009](https://doi.org/10.32614/RJ-2017-009).
- [24] Peter J Brockwell, Peter J Brockwell, Richard A Davis, and Richard A Davis. *Introduction to time series and forecasting*. Springer, 2016.
- [25] Agustín Maravall. "On structural time series models and the characterization of components." In: *Journal of Business & Economic Statistics* 3.4 (1985), pp. 350–355.
- [26] James Durbin and Siem Jan Koopman. *Time Series Analysis by State Space Methods*. Aug. 2001.
- [27] Sean J Taylor and Benjamin Letham. "Forecasting at scale." In: *PeerJ Preprints* 5 (Sept. 2017), e3190v2. ISSN: 2167-9843. DOI: [10.7287/peerj.preprints.3190v2](https://doi.org/10.7287/peerj.preprints.3190v2). URL: <https://doi.org/10.7287/peerj.preprints.3190v2>.
- [28] Andrew C Harvey and Simon Peters. "Estimation procedures for structural time series models." In: *Journal of forecasting* 9.2 (1990), pp. 89–108.

- [29] Trevor Hastie and Robert Tibshirani. “Generalized additive models: some applications.” In: *Journal of the American Statistical Association* 82.398 (1987), pp. 371–386.
- [30] Everette S Gardner Jr. “Exponential smoothing: The state of the art.” In: *Journal of forecasting* 4.1 (1985), pp. 1–28.
- [31] George Evelyn Hutchinson. *An introduction to population ecology*. 504: 51 HUT. 1978.
- [32] Andrew C Harvey and Neil Shephard. “10 Structural time series models.” In: (1993).
- [33] Maurizio Montel. *python-holidays*. <https://github.com/dr-prodigy/python-holidays>. 2021.
- [34] Bob Carpenter, Andrew Gelman, Matthew D Hoffman, Daniel Lee, Ben Goodrich, Michael Betancourt, Marcus A Brubaker, Jiqiang Guo, Peter Li, and Allen Riddell. “Stan: a probabilistic programming language.” In: *Grantee Submission* 76.1 (2017), pp. 1–32.
- [35] Michael Betancourt. *A Conceptual Introduction to Hamiltonian Monte Carlo*. 2018. arXiv: [1701.02434 \[stat.ME\]](https://arxiv.org/abs/1701.02434).
- [36] Matthew D Hoffman and Andrew Gelman. “The No-U-Turn sampler: adaptively setting path lengths in Hamiltonian Monte Carlo.” In: *J. Mach. Learn. Res.* 15.1 (2014), pp. 1593–1623.
- [37] Radford M Neal et al. “MCMC using Hamiltonian dynamics.” In: *Handbook of markov chain monte carlo* 2.11 (2011), p. 2.
- [38] Michel A Cuendet and Wilfred F van Gunsteren. “On the calculation of velocity-dependent properties in molecular dynamics simulations using the leapfrog integration algorithm.” In: *The Journal of chemical physics* 127.18 (2007), p. 184102.
- [39] R. Fletcher. *Practical methods of optimization*. Chichester; New York: Wiley, 1987.
- [40] Priti Mishra and Margaret H Eich. “Join processing in relational databases.” In: *ACM Computing Surveys (CSUR)* 24.1 (1992), pp. 63–113.
- [41] The pandas development team. *pandas-dev/pandas: Pandas*. Version latest. Feb. 2020. DOI: [10.5281/zenodo.3509134](https://doi.org/10.5281/zenodo.3509134). URL: <https://doi.org/10.5281/zenodo.3509134>.
- [42] Hirotugu Akaike. “Information Theory and an Extension of the Maximum Likelihood Principle.” In: *Selected Papers of Hirotugu Akaike*. Ed. by Emanuel Parzen, Kunio Tanabe, and Genshiro Kitagawa. New York, NY: Springer New York, 1998, pp. 199–213. ISBN: 978-1-4612-1694-0. DOI: [10.1007/978-1-4612-1694-0_15](https://doi.org/10.1007/978-1-4612-1694-0_15). URL: https://doi.org/10.1007/978-1-4612-1694-0_15.
- [43] Rob J. Hyndman and Yeasmin Khandakar. “Automatic Time Series Forecasting: The forecast Package for R.” In: *Journal of Statistical Software, Articles* 27.3 (2008), pp. 1–22. ISSN: 1548-7660. DOI: [10.18637/jss.v027.i03](https://doi.org/10.18637/jss.v027.i03). URL: <https://www.jstatsoft.org/v027/i03>.
- [44] K Rantou. “Missing Data in Time Series and Imputation Methods.” In: *University of the Aegean, Samos* (2017).
- [45] Dennis D. Wackerly, William Mendenhall III, and Richard L. Scheaffer. *Mathematical Statistics with Applications*. sixth edition. Duxbury Advanced Series, 2002.
- [46] Cort J Willmott and Kenji Matsuura. “Advantages of the mean absolute error (MAE) over the root mean square error (RMSE) in assessing average model performance.” In: *Climate research* 30.1 (2005), pp. 79–82.
- [47] International Electrotechnical Comission. *Management of alarm systems for the process industries*. 2014.
- [48] Iman Izadi, Sirish L Shah, David S Shook, and Tongwen Chen. “An introduction to alarm analysis and design.” In: *IFAC Proceedings Volumes* 42.8 (2009), pp. 645–650.